SATELLITE & MESOMETEOROLOGY RESEARCH PROJECT

Department of the Geophysical Sciences
The University of Chicago

CLOUD VELOCITIES OVER THE NORTH ATLANTIC COMPUTED FROM ATS PICTURE SEQUENCES

by

Yun-Mei Chang and Jaime J. Tecson

SMRP Research Paper

Number 121
June 1974

MESOMETEOROLOGY PROJECT --- RESEARCH PAPERS

1.* Report on the Chicago Tornado of March 4, 1961 - Rodger A. Brown and Tetsuya Fujita

2.* Index to the NSSP Surface Network - Tetsuya Fujita

3.* Outline of a Technique for Precise Rectification of Satellite Cloud Photographs - Tetsuya Fujita

4.* Horizontal Structure of Mountain Winds - Henry A. Brown

5.* An Investigation of Developmental Processes of the Wake Depression Through Excess Pressure Analysis of Nocturnal Showers - Joseph L. Goldman

6.* Precipitation in the 1960 Flagstaff Mesometeorological Network - Kenneth A. Styber

7.** On a Method of Single- and Dual-Image Photogrammetry of Panoramic Aerial Photographs - Tetsuya Fujita

8. A Review of Researches on Analytical Mesometeorology - Tetsuya Fujita

9.* Meteorological Interpretations of Convective Nephsystems Appearing in TIROS Cloud Photographs - Tetsuya Fujita, Toshimitsu Ushijima, William A. Hass, and George T. Dellert, Jr.

10.* Study of the Development of Prefrontal Squall-Systems Using NSSP Network Data - Joseph L. Goldman

11. Analysis of Selected Aircraft Data from NSSP Operation, 1962 - Tetsuya Fujita

12. Study of a Long Condensation Trail Photographed by TIROS I - Toshimitsu Ushijima

13. A Technique for Precise Analysis of Satellite Data; Volume I - Photogrammetry (Published as MSL Report No. 14) - Tetsuya Fujita

14. Investigation of a Summer Jet Stream Using TIROS and Aerological Data - Kozo Ninomiya

15. Outline of a Theory and Examples for Precise Analysis of Satellite Radiation Data - Tetsuya Fujita

16. Preliminary Result of Analysis of the Cumulonimbus Cloud of April 21, 1961 - Tetsuya Fujita and James Arnold

17. A Technique for Precise Analysis of Satellite Photographs - Tetsuya Fujita

18.* Evaluation of Limb Darkening from TIROS III Radiation Data - S.H.H. Larsen, Tetsuya Fujita, and W.L. Fletcher

19. Synoptic Interpretation of TIROS III Measurements of Infrared Radiation - Finn Pedersen and Tetsuya Fujita

20.* TIROS III Measurements of Terrestrial Radiation and Reflected and Scattered Solar Radiation - S.H.H. Larsen, Tetsuya Fujita, and W.L. Fletcher

21. On the Low-level Structure of a Squall Line - Henry A. Brown

22.* Thunderstorms and the Low-level Jet - William D. Bonner

23.* The Mesoanalysis of an Organized Convective System - Henry A. Brown

24. Preliminary Radar and Photogrammetric Study of the Illinois Tornadoes of April 17 and 22, 1963 - Joseph L. Goldman and Tetsuya Fujita

25. Use of TIROS Pictures for Studies of the Internal Structure of Tropical Storms - Tetsuya Fujita with Rectified Pictures from TIROS I Orbit 125, R/O 128 - Toshimitsu Ushijima

26. An Experiment in the Determination of Geostrophic and Isallobaric Winds from NSSP Pressure Data - William Bonner

27. Proposed Mechanism of Hook Echo Formation - Tetsuya Fujita with a Preliminary Mesosynoptic Analysis of Tornado Cyclone Case of May 26, 1963 - Tetsuya Fujita and Robbi Stuhmer

28. The Decaying Stage of Hurricane Anna of July 1961 as Portrayed by TIROS Cloud Photographs and Infrared Radiation from the Top of the Storm - Tetsuya Fujita and James Arnold

29. A Technique for Precise Analysis of Satellite Data, Volume II - Radiation Analysis, Section 6. Fixed-Position Scanning - Tetsuya Fujita

30. Evaluation of Errors in the Graphical Rectification of Satellite Photographs - Tetsuya Fujita

31. Tables of Scan Nadir and Horizontal Angles - William D. Bonner

32. A Simplified Grid Technique for Determining Scan Lines Generated by the TIROS Scanning Radiometer - James E. Arnold

33. A Study of Cumulus Clouds over the Flagstaff Research Network with the Use of U-2 Photographs - Dorothy L. Bradbury and Tetsuya Fujita

34. The Scanning Printer and Its Application to Detailed Analysis of Satellite Radiation Data - Tetsuya Fujita

35. Synoptic Study of Cold Air Outbreak over the Mediterranean using Satellite Photographs and Radiation Data - Aasmund Rabbe and Tetsuya Fujita

36. Accurate Calibration of Doppler Winds for their use in the Computation of Mesoscale Wind Fields - Tetsuya Fujita

37. Proposed Operation of Intrumented Aircraft for Research on Moisture Fronts and Wake Depressions - Tetsuya Fujita and Dorothy L. Bradbury

38. Statistical and Kinematical Properties of the Low-level Jet Stream - William D. Bonner

39. The Illinois Tornadoes of 17 and 22 April 1963 - Joseph L. Goldman

40. Resolution of the Nimbus High Resolution Infrared Radiometer - Tetsuya Fujita and William R. Bandeen

41. On the Determination of the Exchange Coefficients in Convective Clouds - Rodger A. Brown

* Out of Print
** To be published

(Continued on back cover)

CLOUD VELOCITIES OVER THE NORTH ATLANTIC COMPUTED FROM ATS PICTURE SEQUENCES

by

Yun-Mei Chang and Jaime J. Tecson
Department of the Geophysical Sciences
The University of Chicago

SMRP Research Paper No. 121

June 1974

Research supported by the Atmospheric Sciences Section, National Science Foundation, NSF Grant GA-41845.

CLOUD VELOCITIES OVER THE NORTH ATLANTIC COMPUTED FROM ATS PICTURE SEQUENCES

Yun-Mei Chang and Jaime J. Tecson
Department of the Geophysical Sciences
The University of Chicago

ABSTRACT

Cloud velocities are obtained in two levels over the North Atlantic area from sequences of ATS-III pictures for eleven days in July 1969 during the BOMEX phase IV experiment. Over 800 cloud vectors are calculated for each day. Detailed high- and low-level flows are analyzed by using computed cloud motion data and observed 200 mb heights and winds. A model is developed for analyzing the high-level outflow from overshooting cloud tops based on thermodynamics and statistics. Results are compared with synoptic observations. It is found that the cloud data reveal various motions in different scales, and it can be concluded that in spite of the scarcity of observations over the tropical area, especially over the ocean areas, the tropical circulations can be described through the cloud motions much more accurately and realistically than have before been possible.

1. INTRODUCTION

Since meteorological satellite pictures have become available and various techniques for analyzing them have been developed, satellite data, among others, have confirmed previously formulated theories concerning circulation in the tropics. The cloud motion, observed from the time-lapse sequences of satellite photographs, reveals not only the large-scale flow patterns but also the life cycle of various types of synoptic-scale disturbances as well as the intensity, frequency and size of sub-synoptic circulation systems.

Recently, it has been possible to utilize ATS satellite photographs to construct flow fields at levels which contain traceable cloud elements. Velocities of tracer clouds have been calculated by a number of people. Among others, the motions of tropical clouds near Hawaii had been computed by Fujita, Murino et al. (1968). By tracking cumulus cells in ATS pictures, flow patterns over the equatorial east Pacific were obtained by Fujita, Watanabe and Izawa (1969) while the flow patterns over the northern tropical Atlantic were obtained by Fujita (1970). Black and Anthes (1971) investigated the cirrus clouds over the tropical cyclone outflow layer by using ATS-III pictures and studied the relevant eddy transport of angular momentum in the hurricane area. Along this line, Gaby and Poteat (1973) derived the low-level winds from the cloud displacements on ATS-III pictures.

With the development of the METRACOM system of cloud velocity computation at SMRP, University of Chicago, a large number of experimental computations have been made. In this study, the North Atlantic Ocean covering the area from 0° -35° N and 25° -80° W has been selected as the area of analysis. Careful manual tracking of high- and low-level clouds from ATS-III sequences of pictures have been done for eleven days during the BOMEX Fourth Phase (July 11-28, 1969). The cloud velocities have been calculated through the IBM 360/168 computer facility at the University. Streamlines for the low-cloud level and contour heights at 200 mb for the high-cloud level are drawn separately by using the calculated cloud velocity vectors together with a few upper-air observations and the relevant aircraft-reported winds. Detailed analyses are attempted on high-level overshooting outflow which existed over the region with strong low-level convection near the equator. A model of the overshooting outflow is developed in an attempt to better understand and portray the circulation patterns over the tropics.

It should be noted that no adjustments have been made to fit the computed cloud velocities with observed winds. Therefore, the cloud velocity patterns presented in this paper should be considered as direct output through calculation of cloud motion field from geostationary satellite data.

2. METHOD OF COMPUTATION

A sequence of ATS-III satellite pictures, which is made into a movie loop, is

used for each day. The period covers about one hour and involves four to five frames of photographs. Since the 2-mile size or larger cumulus cells are suitable target clouds and considering that they are more stable over water as suggested by Fujita et al. (1973), a movie loop period of one hour or a few minutes longer is definitely less than the cloud lifetime. The dissipation effect of the clouds is thus avoided. The movie loop, when projected on a loop projector, displays the cloud motion on the screen. A trained meteorologist can thus identify the flow patterns, distinguish the cloud levels and trace the cloud motions.

To compute the cloud velocity, an electronic digitizer and, subsequently, a computer are used. After the cloud motion vector has been traced from the movie loop, the x-y coordinates of the beginning and end points of the cloud vector are directly read out from the digitizer and automatically punched into data cards. The graphical data are thus converted into digital form for computer applications. As shown in Fig. 1,

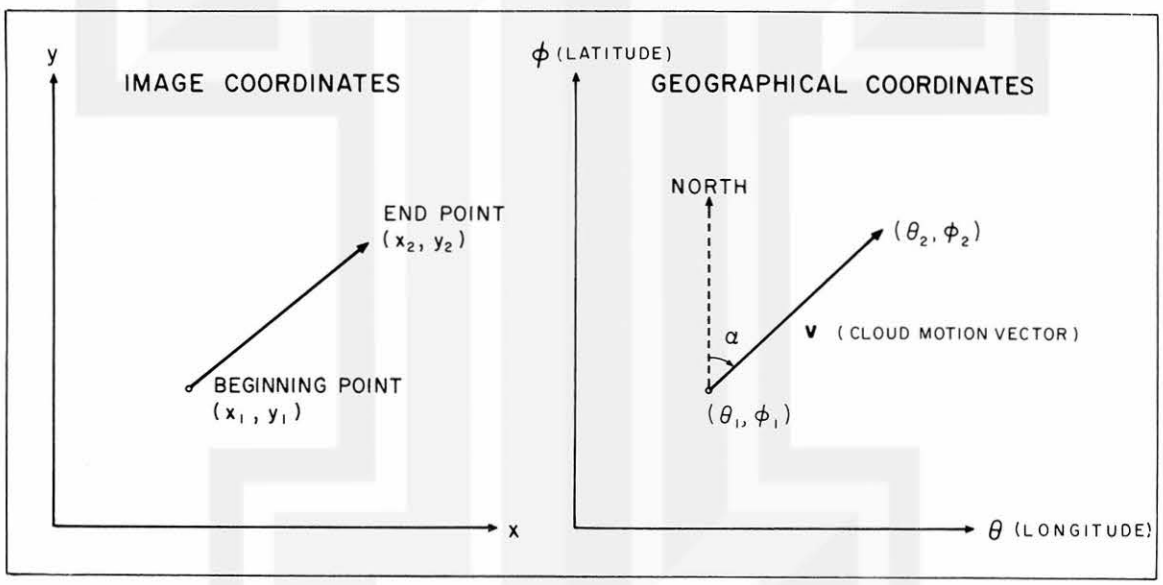

Fig. 1. Left: A tracked cloud velocity vector in image coordinate (x,y) with beginning point (x_1, y_1) and end point (x_2, y_2). Right: The cloud motion vector in geographical coordinate (θ, ϕ) with azimuth (α) and magnitude (v).

the graphical coordinates of each vector in the image coordinates (x,y) are transformed to the geographical coordinates, namely, the latitude (ϕ) and longitude (θ). The azimuth (α) and magnitude (v) of each cloud vector are thus calculated. For detailed

discussion of the method, see the report on METRACOM system by Chang et al. (1973). The computations under this system permit an accuracy to within 1 meter per second in speed and 4 degrees in direction as investigated by Fujita et al. (1973).

In this study, cloud motions for eleven days in July 1969 have been tracked and calculated. Extreme care has been taken in the selection of cloud tracers and the determination of high and low clouds. In general, the low clouds are mainly the cumuliform types. They form as cloud clusters that show up distinctly as small spots. Figure 2 is an example of some traced low cumulus cloud vectors and their flow pattern. High clouds are mainly cirriform clouds which appear in the movie loop as

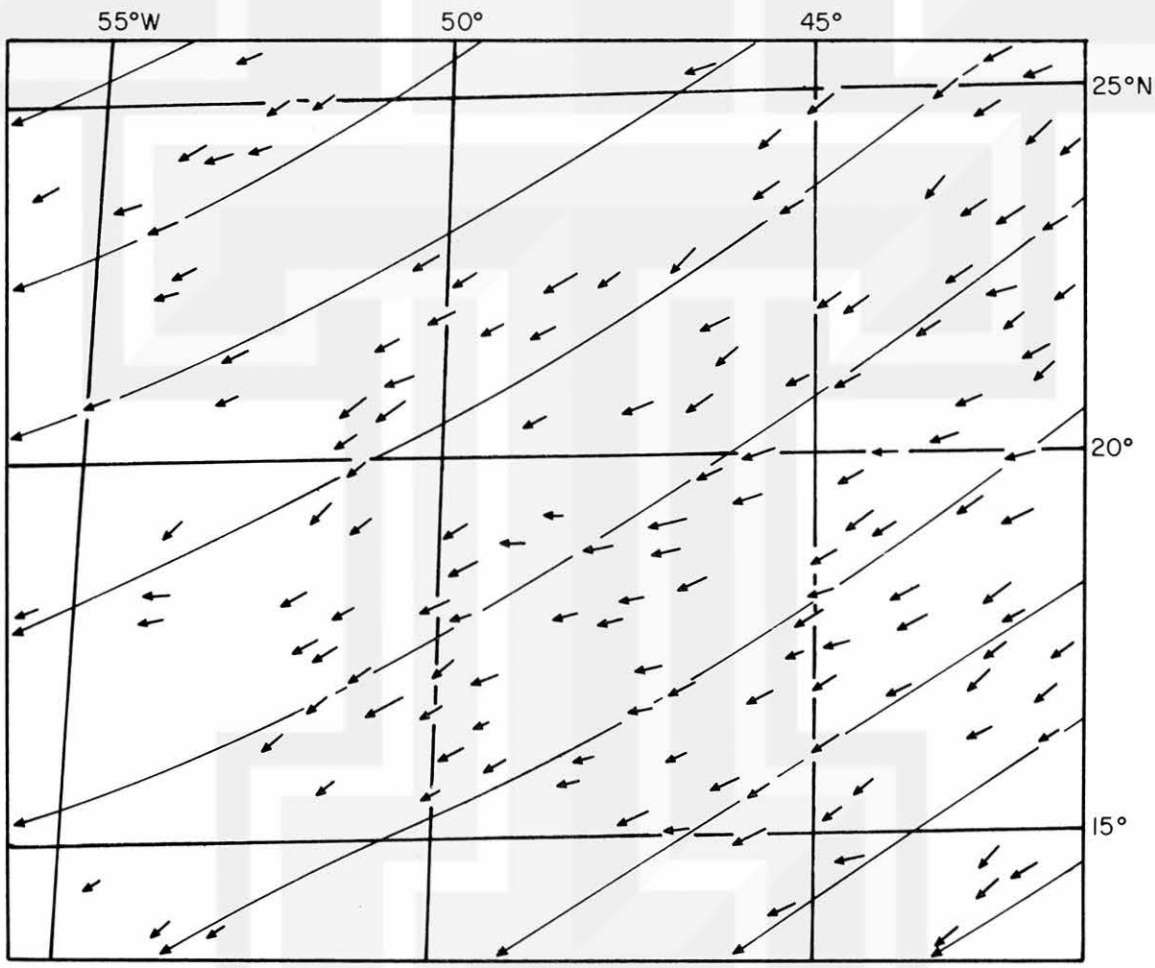

Fig. 2. Motion of low clouds shown as arrows as seen on an ATS III movie loop for 1350-1454 GMT, July 26, 1969. Approximate flow pattern is superimposed.

bright and fuzzy with hazy boundaries. Either they cover a large area and move as a whole or appear as the cirrus anvils spreading out from the overshooting towering

cumulus tops. The high clouds are tracked separately from the low clouds so as to distinguish their different motion fields. An example of diverging pattern in the high cloud is shown in Fig. 3.

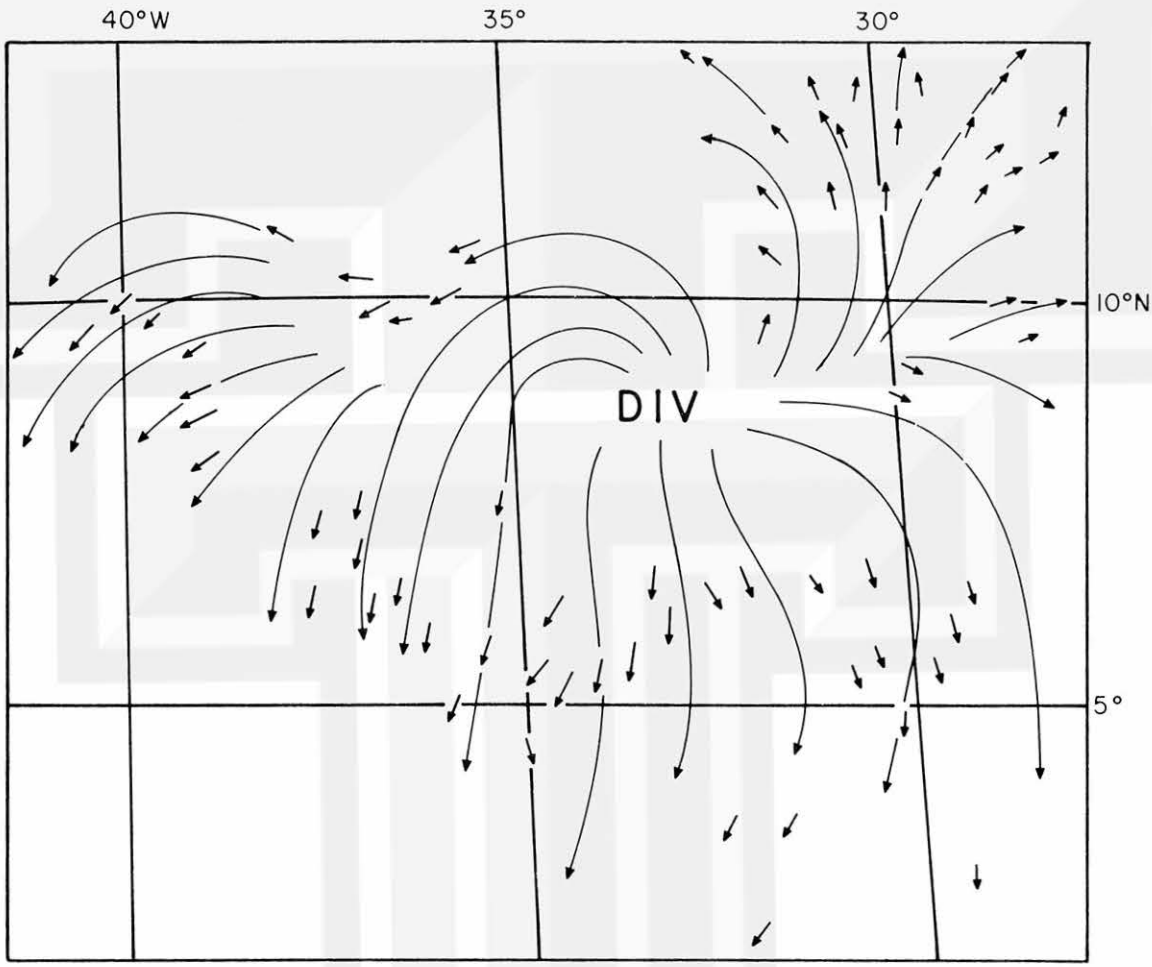

Fig. 3. Motion of high clouds shown as arrows as seen on an ATS III movie loop for 1350-1454 GMT, July 26, 1969. Approximate flow pattern is superimposed.

3. ANALYSIS OF LOW-LEVEL FLOW

Figure 4 is a streamline analysis of the computed low-level cloud motion vectors for 1350-1454 GMT, July 26, 1969. The area extends approximately from 0° N to 35° N and 25° W to 80° W. The shaded areas indicate the high clouds. There are tremendously sufficient low-cloud tracers over the North Atlantic Ocean, especially in the northeast quadrant of the area. A uniform northeasterly flow curves anticyclonically around a high pressure center located over the northern portion of the region.

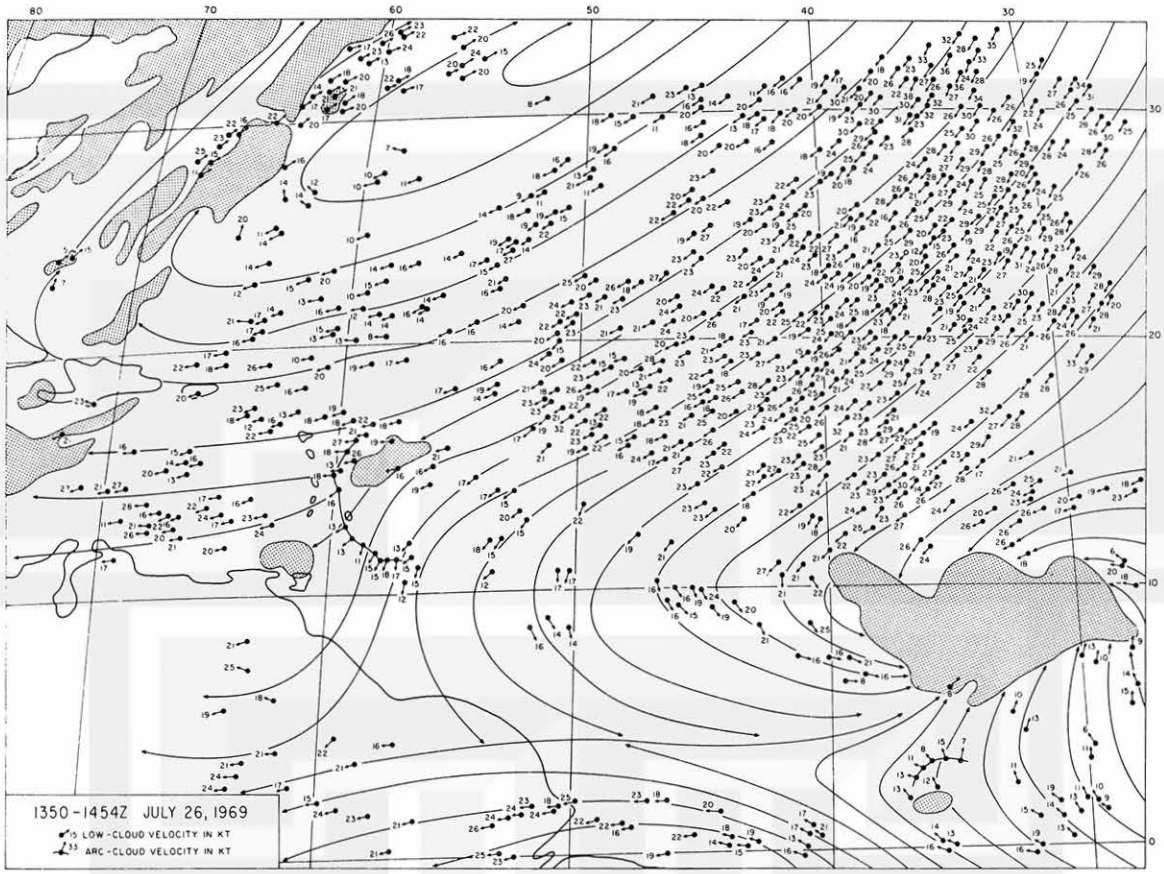

Fig. 4. Velocity vectors of low clouds over the Atlantic Ocean for July 26, 1969. A sequence of six pictures taken between 1350 and 1454 GMT is used for the computation. Cloud elements in an arc cloud are connected with a heavy line. High cloud areas are shaded. Flow patterns are shown with streamlines drawn to fit cloud velocities.

A strong cyclonic motion with high cirrus cloud cover dominates the area east of 42° W and south of 14° N; this corresponds to the developing storm Anna which was analyzed and tracked as a weather system by Fernandez-Partagas and Estoque (1970). Strong inflow converging to the cyclone center produces strong upward motion in this area. Convergent motion is also found in the other area near the tropics, namely, the region covered with high clouds centered about 15° N and 58° W. A shear line formed near the equator, at about 5° N, is shown as a result of the converging motion of the northerly flow into the cyclonic circulation and the southeast equatorial flow. These low-level convergent motions, which exist usually from 5° N to 15° N, represent a zone of concentrated convection and appear as a cloud band on the satellite photographs. This equatorial cloud band, known as ITCZ, is one of the striking features of cloud organization in the tropics.

Two arc clouds are shown, each as a string of cloud motion vectors connected by a heavy line. One is located in the vicinity of 13° N and 60° W moving away from the high cloud area east of it. Another is found around 2° N and 36° W moving away from the high cloud area south of it. These arc-shaped clouds move quite rapidly without changing their shape. The movement of arc clouds may represent a certain kind of small-scale flow or motion of a meso-front. Further investigations on them are being made.

The low-level cloud motion thus calculated and analyzed are compared with the observed winds at the surface and at 3000 ft at 1200 GMT. It is observed that the cloud motion could represent the 3000 ft flow pattern quite well except that the magnitudes of the cloud velocities are stronger than the observed winds. It may be remarked that the cloud motion over land areas near the equator are harder to track and conform less with the 3000-ft winds, and to an even lesser degree with the surface winds. The more accurate determination of cloud heights is hopefully expected to be achieved after more infrared data become available.

4. ANALYSIS OF HIGH-LEVEL FLOW

The distribution of the high-level cloud motion vectors for the same time, date and area in Fig. 4 is shown in Fig. 5. The streamline analysis on the expanding high clouds is drawn superimposed on the contour height analysis of the high-level flow. The shaded area, as mentioned before, is the area covered by the high cirrus clouds. The contour height analysis of high-level flow is done by using the high-cloud motion vectors together with the observed 200 mb winds and heights at 1200 GMT and the relevant aircraft winds. The synoptic wind data at 200 mb are plotted in the conventional form. The selection of 200 mb level is made considering that this could be the nearest level for the outflow of the overshooting cloud tops. A model for obtaining the height over the overshooting outflow area is discussed in the next section.

The cloud motions in Fig. 5 clearly indicate that superimposed on the large-scale high-level flow, some disturbed flow, which is characterized by the upper-divergence fields, is closely related to the location of high cirrus clouds. Two significant regions of upper-divergence exist at this time; one occupies a large area of high cloud near 9° N and 34° W, and the other is in the cloud clusters near the island of

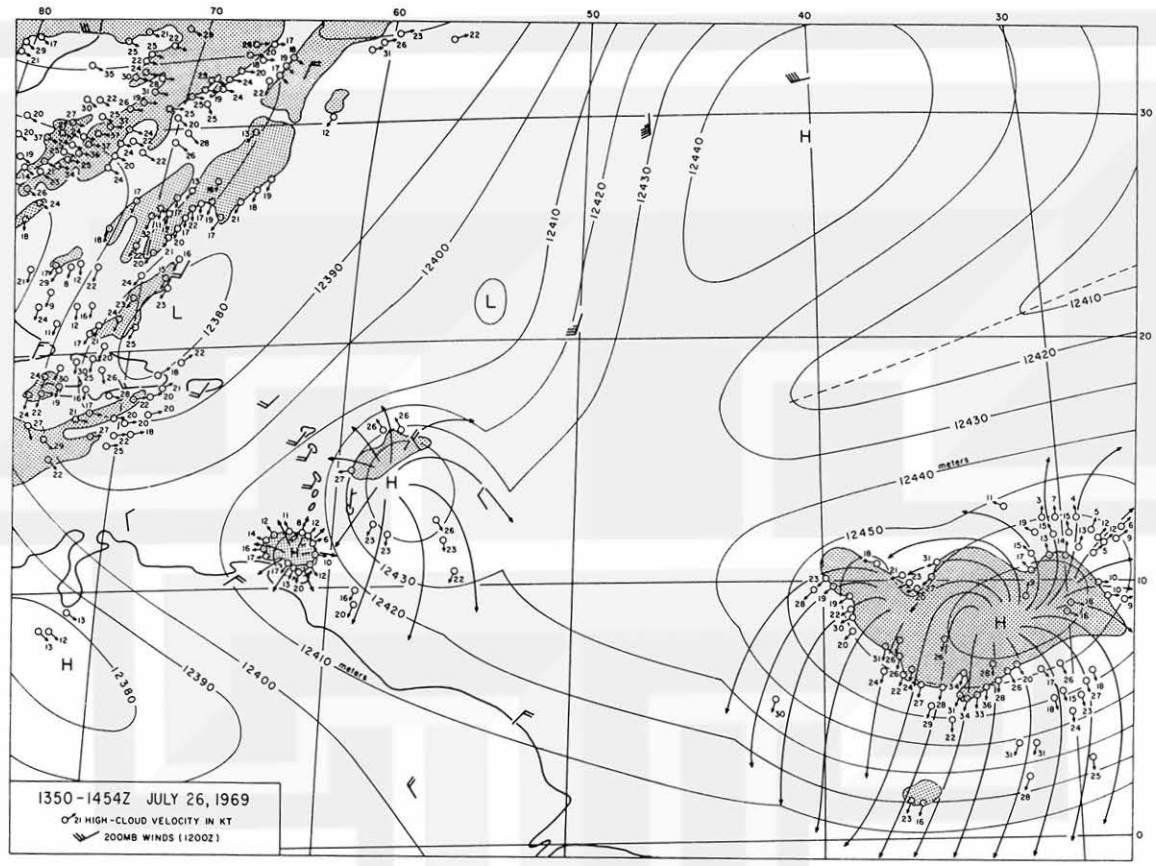

Fig. 5. Velocity vectors of high clouds for the same area shown in Fig. 4 during the same period. Contour lines are drawn using the cloud velocity vectors and the observed 200 mb wind and height data. Streamlines for the expansion high clouds (shaded area) are superimposed.

Barbados. The large-scale high-level flow patterns are modified by these diverging high clouds. The large diverging area near 34° W has predominantly anticyclonic outflow. This is associated with the clouds comprising the tropical disturbance which has marked inflow in the lower level as shown in Fig. 4. The high-level outward propagating cloud bands in hurricane areas have been produced in a numerical model by Kurihara and Tuleya (1974) who have suggested that these cloud bands behave similar to internal gravity waves. The outflow shown in Fig. 5 curves away from the equator, due to the Coriolis effect, but becomes non-curvature flow as it approaches the equator.

Near the island of Barbados, there are two anticyclones associated with the two upper-diverging high-cloud clusters. Cirrus anvils spread out from towering cumulus. Again, for the smaller area of the expansion cloud, without the considerable effect of Coriolis force, the flow is non-curvature; however, for the larger area of the expansion cloud, the flow turns anticyclonically.

The existence of an upper outflow field appears mostly in the ITCZ region. The strong upward motion due to the concentrated convectivity at low level leads to the overshooting outflow at higher level. This penetrating anvil top evidently plays a significant role in the tropical circulations.

5. ANALYSIS MODEL OF OVERSHOOTING OUTFLOW

The outflow from overshooting cloud tops, or overshooting outflow, which can be seen from satellite photographs has been investigated by many people. Detailed analysis on overshooting thunderheads has been done by Fujita (1974) by using pictures both from ATS and Learjet flights at high altitudes. As discussed in Section 4, the spreading high clouds are found over the tropical regions, where the strong low-level convection exists. The horizontal dimensions vary between 200 km and 3000 km, which consist of several overshooting clouds of various sizes. As shown in Fig. 6, several anvil clouds develop from the tops of tall convective clouds; the strong updraft causes them to pass the crossover point and reach the overshooting top. A maximum overshooting height of 2 km is assumed from observation. Cirrus clouds then spread out from the overshooting clouds. The crossover point could be higher or lower than the tropopause.

The overshooting from an anvil top comprises a series of four stages as shown in Fig. 7; namely, the development stage, the mature stage, the spreading stage, and the dissipation stage. The strong updraft triggers the overshooting thus starting the development stage. Continuously gaining in kinetic energy, stronger updrafts bring the cloud to its highest point which is the mature stage. From then on, the cirrus spreads out from the anvil top, called the spreading stage, and finally, because of the dissipation of the energy, the updraft becomes weaker and weaker, the overshooting flattens out and reaches its dissipation stage.

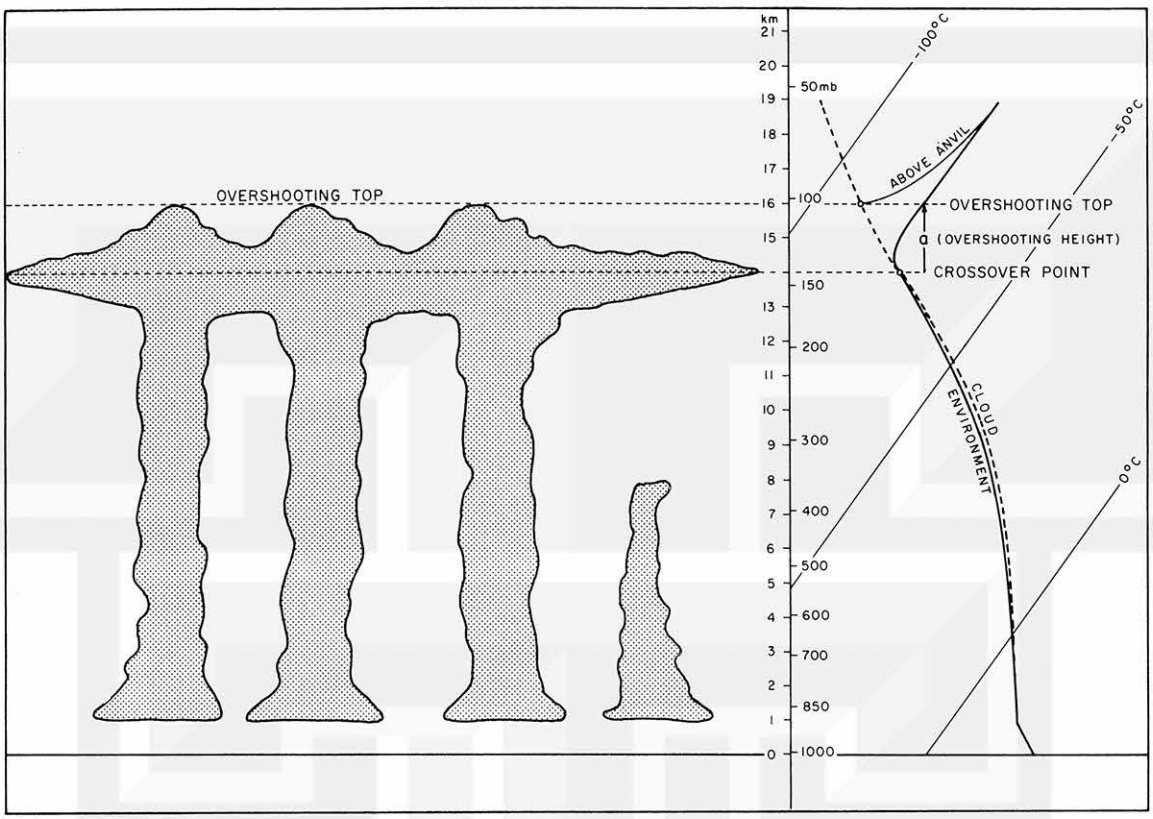

Fig. 6. A group of anvil clouds with overshooting height, a. The vertical temperature profiles for the cloud (moist adiabatic) and the environmental air are indicated at the right portion of the figure.

Statistically, the maximum overshooting height can be expressed as an exponential decay function of its radius. This can be computed from the following equation

$$\frac{A_R}{A_{Rm}} = C(1 - e^{-nkR})e^{-kR} , \qquad C \equiv \frac{e^{kRm}}{1 - e^{-nkRm}} \qquad (1)$$

where Rm is the radius of an overshooting outflow at its maximum height; A_R and A_{Rm} are the overshooting heights at the center of the overshooting clouds with radius R and Rm, respectively; n and k are constants. For $Rm = 500$ km which is the case in this study, the normalized overshooting height A_R/A_{Rm} is shown in Fig. 8 for different n and k. Here, $n = 1$ and $k = 0.00139$ are used.

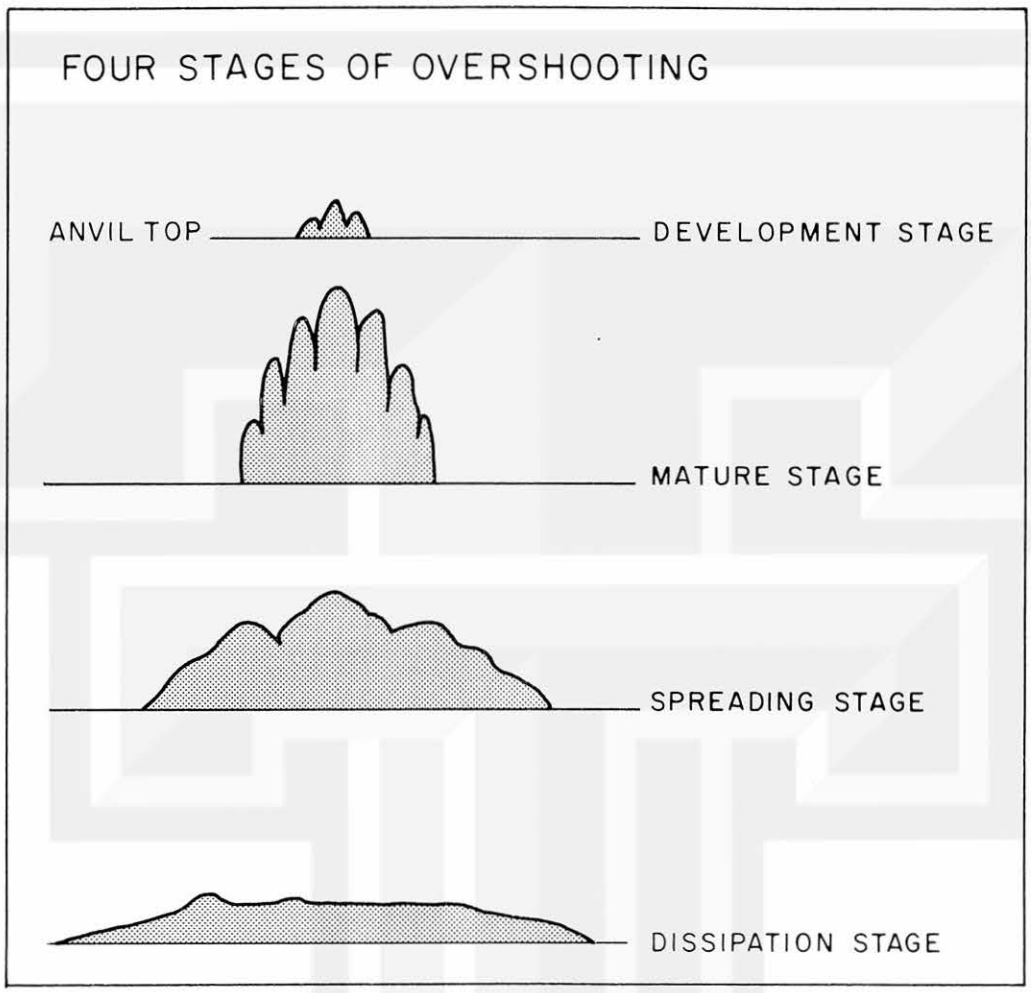

Fig. 7. The four stages of overshooting cloud from the anvil top.

Following Fujita (1974), a dome shape of overshooting outflow is assumed. With the aid of Fig. 9, the dome can be represented as the upper part of a cosine curve. The overshooting height, a , at any radius, r , can be expressed as

$$a = 2A_R\left(-\frac{1}{2} + \cos\frac{r}{R}\frac{\pi}{3}\right) \qquad (2)$$

provided $r \leq R$ and A_R and R are defined in Eq. (1).

Due to the presence of cold air aloft, an excess hydrostatic pressure over the overshooting cloud top exists. This can be calculated from the hydrostatic balance equation, namely,

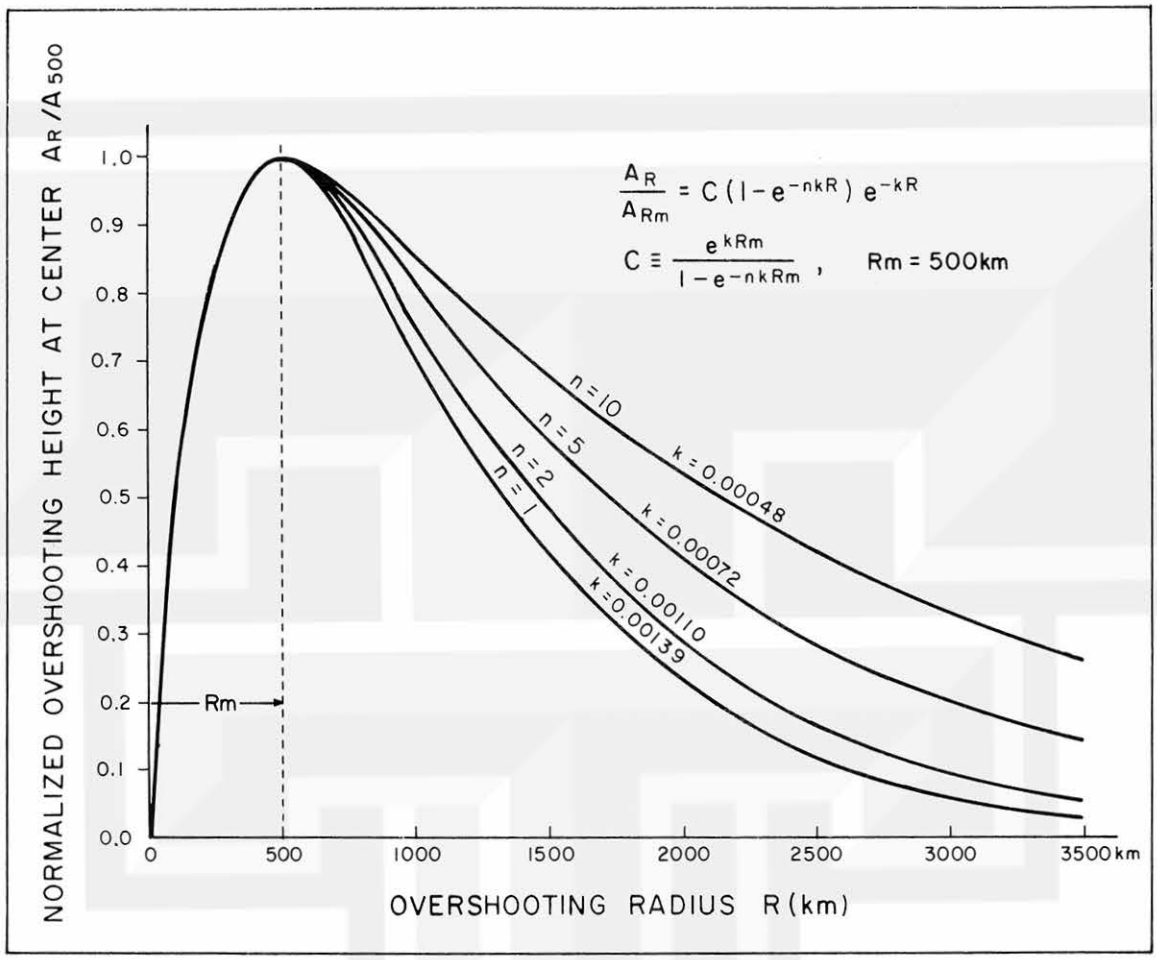

Fig. 8. A statistical model for overshooting cloud height at center, A_R, with the maximum overshooting height at $Rm = 500$ km, where R denotes the radius of the overshooting.

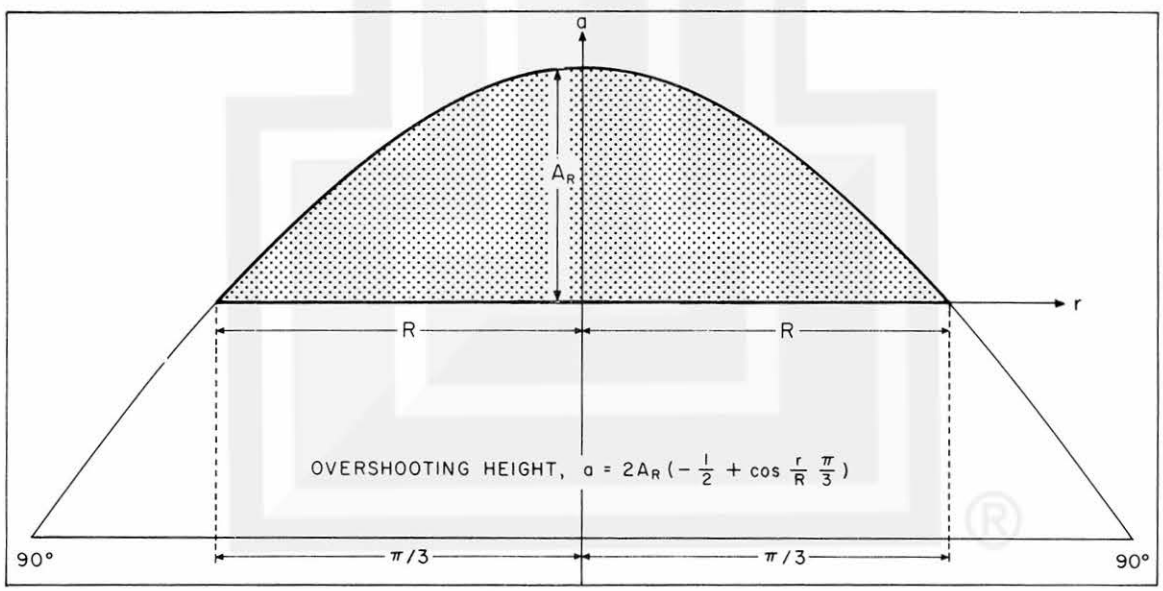

Fig. 9. A dome-shaped overshooting cloud (shaded area) with radius R and center height, A_R. The dome is the upper portion of a cosine curve.

$$\frac{dP}{P} = -\frac{g}{\bar{R}T}\,dz \tag{3}$$

where the pressure, P, and temperature, T, are at height z; $\bar{R}$ and g are the gas and gravitational constants, respectively.

If P_0 represents the pressure at the crossover point, then, by integrating Eq. (3), the pressure for the surrounding air, P_1, and for cloud top, P_2, at overshooting height, a, can be written as

$$P_1 = P_0\, e^{-\frac{g}{\bar{R}T_1}a} \tag{4}$$

$$P_2 = P_0\, e^{-\frac{g}{\bar{R}T_2}a} \tag{5}$$

where T_1 and T_2 are the temperatures corresponding to P_1 and P_2, respectively, which are obtained from the sounding data. Then, the excess hydrostatic pressure at the overshooting cloud top is

$$\Delta P = P_2 - P_1 = P_0\left[e^{-\frac{ga}{\bar{R}T_2}} - e^{-\frac{ga}{\bar{R}T_1}}\right] \tag{6}$$

Figure 10 is a plot for ΔP with respect to overshooting height, a, by taking a sounding in the rain area of hurricanes (from Riehl, 1954) as the surrounding air together with moist adiabatic lapse rate as the overshooting cloud.

Hence, for each overshooting outflow with radius R, which is obtained from tracking high cloud motion from sequences of ATS pictures, equations (1) and (2) give the overshooting height, a, at any radius, r. The excess hydrostatic pressure ΔP, at this overshooting height, a, can be obtained from Fig. 10 or Eq. (6), and then, the height, z, at r can thus be calculated from the following hydrostatic balance equation

$$\Delta z = z - z_0 = -\frac{1}{\rho g}\Delta P \approx -\frac{\bar{R}}{gP_0}T\,\Delta P \tag{7}$$

and

$$z = z_0 - \frac{\bar{R}}{gP_0}T\,\Delta P \tag{8}$$

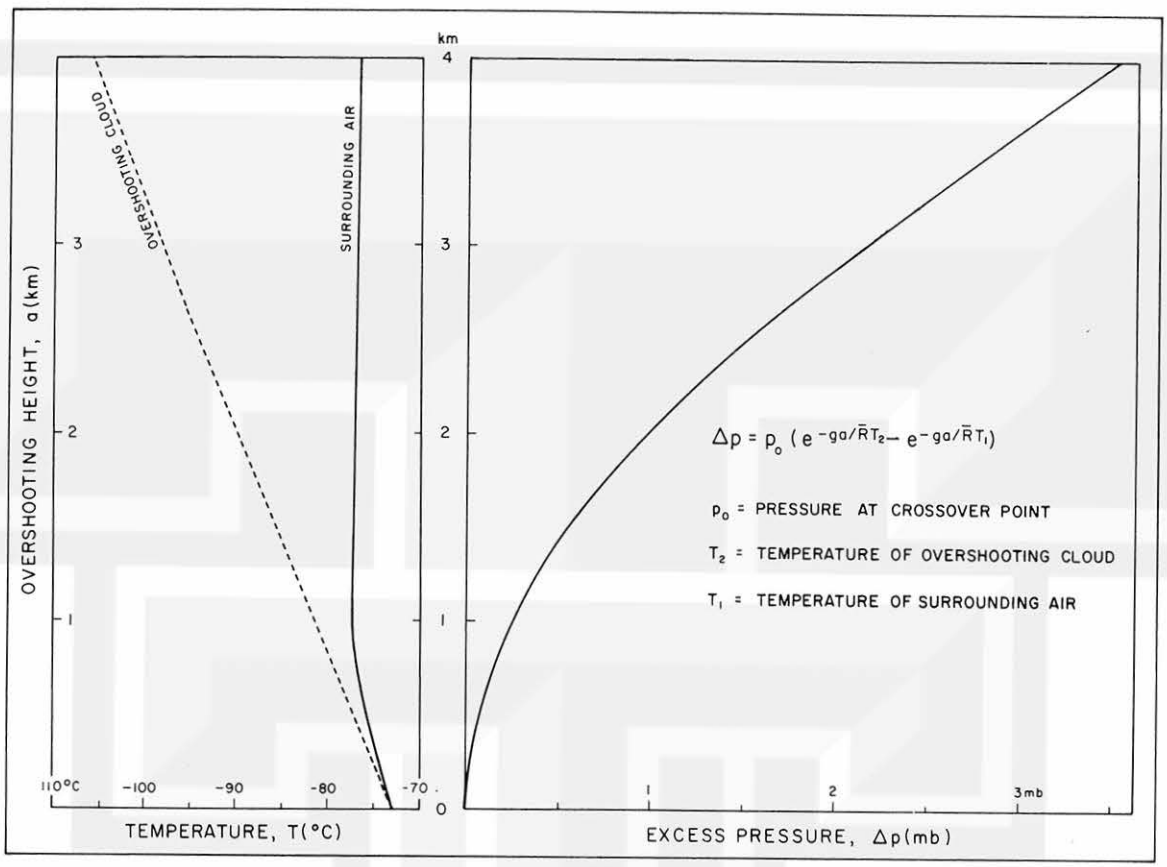

Fig. 10. Left: The soundings for the surrounding air (from Riehl, 1954, p. 314) and for the overshooting cloud (moist adiabatic). Right: The corresponding excess hydrostatic pressure, Δ p (mb) for the overshooting cloud.

where z_o is the height at crossover point, T is the temperature at height z , and ρ is the density.

Patterns of contour height analyses at high-levels where overshooting outflows are observed from satellite photographs are shown in simplified form in Figs. 11 and 12. Typical outflows appear to be mostly circular or elliptical in shape, although other configurations do occur. Figure 11, top portion, shows the resultant contour analysis for a circular-shaped outflow with arbitrary spacing between isohypses. N is any arbitrary reference height at 200 mb level. The bottom portion shows the analysis for the same outflow configuration but with closer spacings between isohypses. Similarly, analysis of elliptical-shaped outflow is depicted in Fig. 12 with the top portion characterized by wider spacings between isohypses than that in the bottom portion.

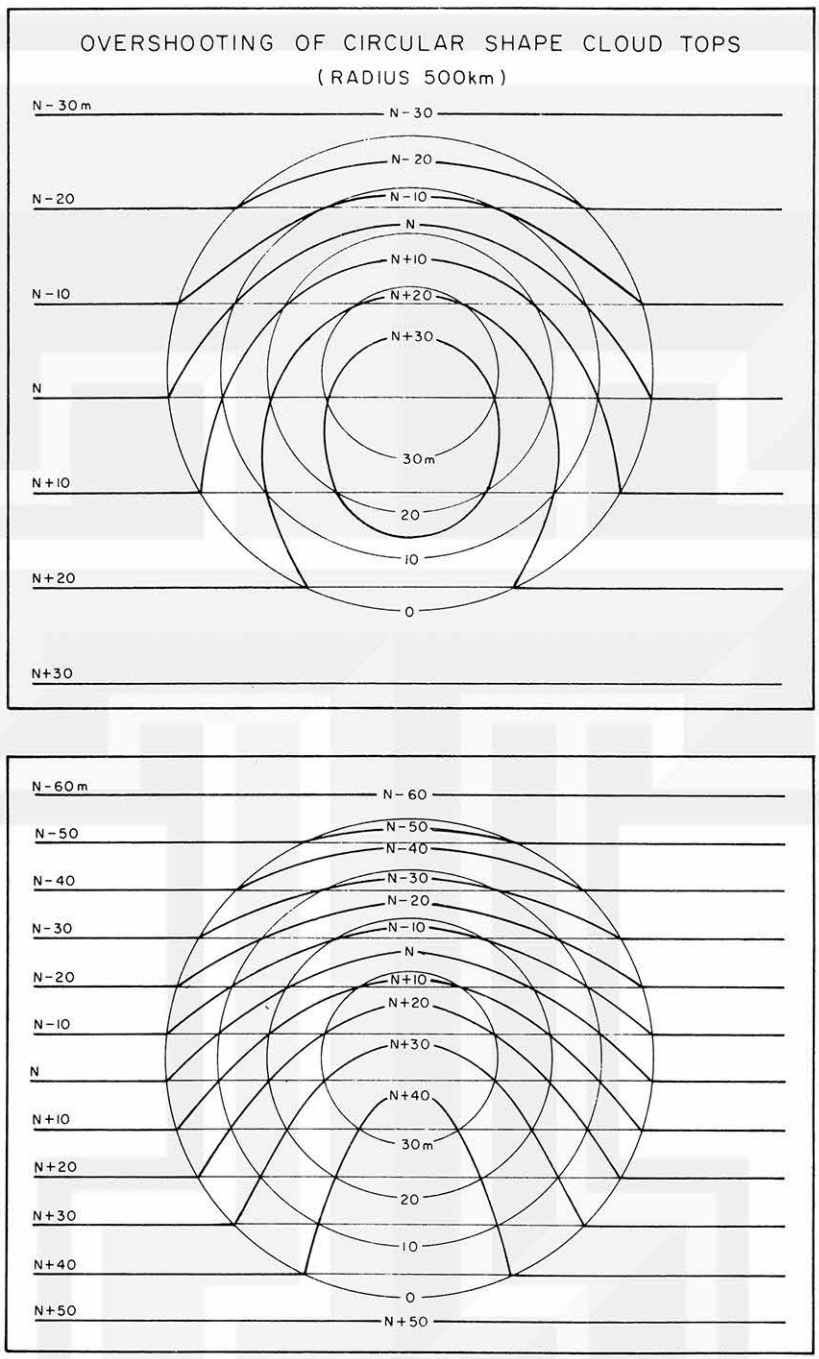

Fig. 11. Examples of circular-shaped overshooting clouds with radius 500 km in two different contour gradients. The thin concentric lines are the contours for the overshooting clouds. The thick lines are the resultant contours in the large-scale flow. N is any arbitrary reference height in meters at the 200 mb level.

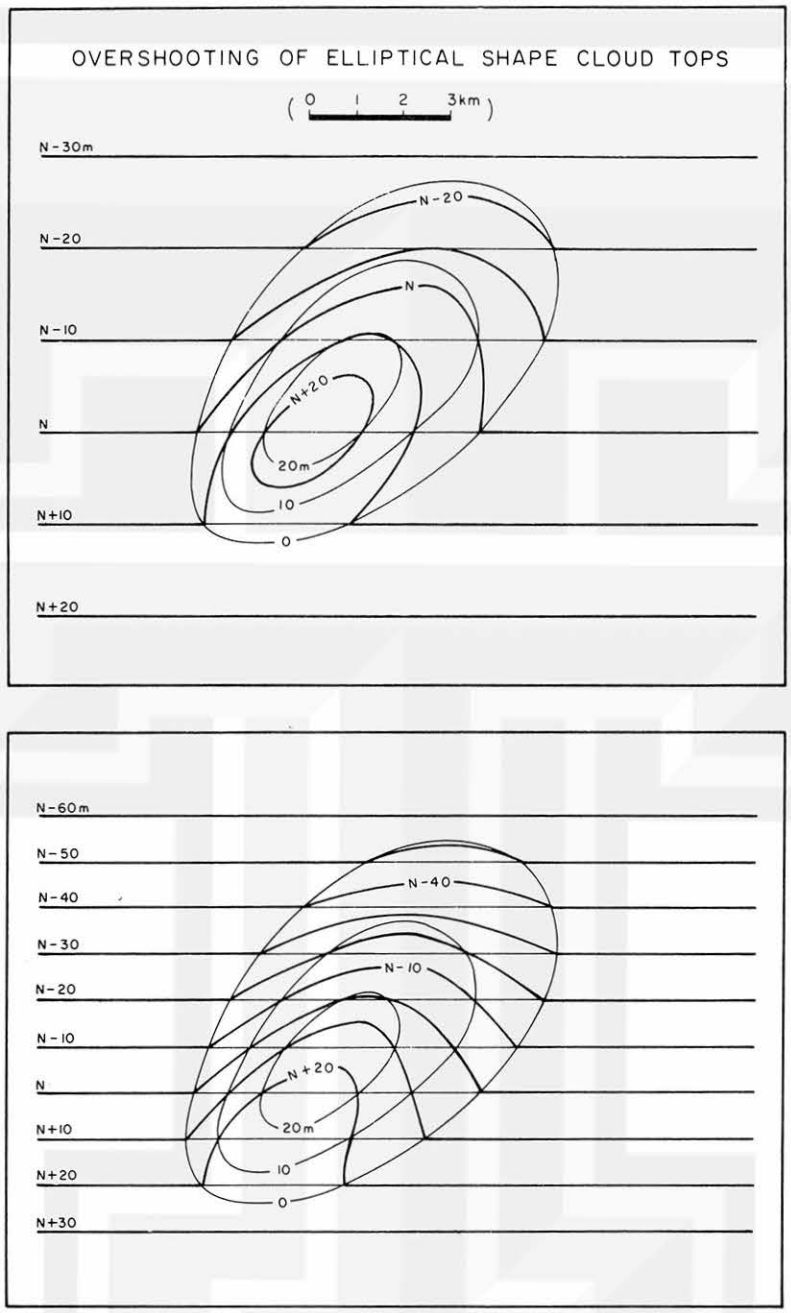

Fig. 12. Examples of elliptical-shaped overshooting clouds in two different contour gradients. The thin elliptical lines are the contours for the overshooting clouds. The thick lines are the resultant contours in the large-scale flow. N is any arbitrary reference height in meters at the 200 mb level.

6. RESULTS OF ANALYSES

The cloud motion analyses from ATS-III pictures for July 11, 12, 13, 15, 17, 22, 23, 24, 27, 28, 1969 are shown in Fig. 13 through 32 (The analyses for July 26, 1969 are presented in Figs. 4 and 5). The area covered is approximately from 0°N to 35°N and 25° W to 80° W. The flow patterns are depicted in two levels. Streamline analyses are drawn for low-level flow and contour height analyses for high-level flow. On the low-level flow charts, the line of clouds connected by a heavy line is an arc cloud, which has been discussed in Section 2. On the high-level flow charts, the computed cloud vectors are plotted together with the observed winds at 200 mb for the nearest 1200 GMT synoptic hour and with whatever relevant aircraft winds. The areas of high clouds are shaded. Streamline analyses are also done on the expansion high clouds. Except for the regions over the South American continent and the area covered by high clouds, the low cloud tracers are abundant in the area under study. For the high-level clouds, cloud tracers are usually found over the upper divergent area and north and west of 15°N and 64° W in the vicinity east of the southern United States. Beyond this region and the outflow area, few cirrus clouds are found. Altogether, between 800 and 1100 cloud vectors are calculated and plotted for each day.

In addition to the large-scale flow patterns, there are two prominent systems in the tropical area that are seen from this series of cloud motion analyses. One is tropical storm Anna which is seen on July 26, 27, 28 and the other is the cloud band comprising the ITCZ. Detailed analyses of the cloud motions show strong low-level cyclonic inflow and high level anticyclonic outflow over the areas of the disturbances.

7. CONCLUSIONS

The facility and accuracy with which numerous cloud motions observed from ATS picture sequences can be quantitatively reduced using the METRACOM system make it practicable to analyze any desired series on a day-to-day basis for cloud velocity determination. For the trained meteorologists, low- and high-level clouds are easily distinguishable by knowing the various cloud configurations and by flow pattern recognition. Two such levels are thus drawn and analyzed. Analysis of low-level flow has revealed a convergence field indicative of low-level convection.

Analysis of high-level flow has indicated the detection of divergence fields, of a nature called overshooting outflow, imbedded in the large-scale circulation. These are normally associated with some active low-level convergence especially in the areas of the ITCZ and tropical disturbances. A model is developed for such overshooting outflow from an anvil top and under certain assumptions, the overshooting heights at any radius can be calculated. Patterns of contour height analyses at high-levels influenced by the overshooting outflows are shown. The four stages of overshooting from an anvil top is discussed.

The results of the cloud-motion analyses indicate that, in addition to supplementing wind-flow patterns over data-sparse regions, mostly over the oceans, they have revealed an interesting aspect whereby high-level overshooting outflow could be detected and tracked. Further cloud motion studies from satellite photographs and more realistic interpretation would certainly contribute to a better understanding of the atmospheric circulation, especially over the tropics.

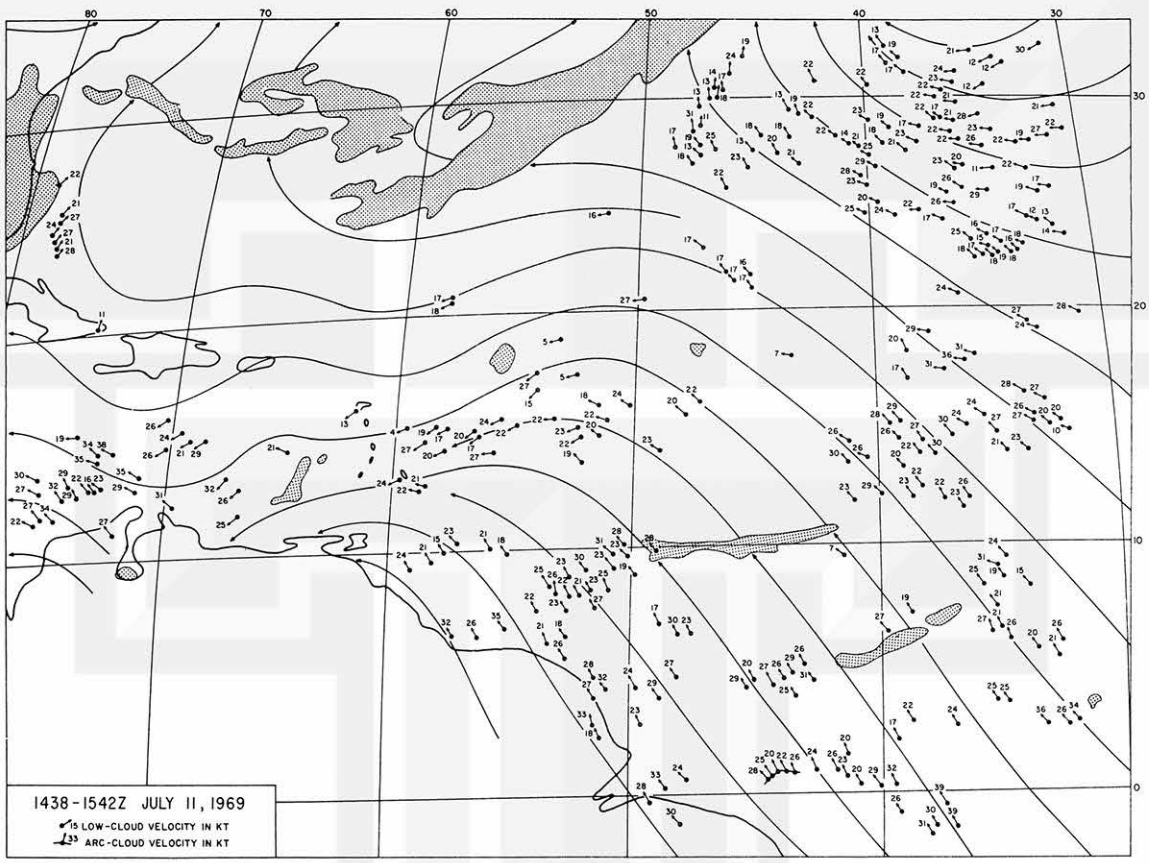

Fig. 13. Velocity vectors of low clouds over the Atlantic Ocean for July 11, 1969. A sequence of six pictures taken between 1438 and 1542 GMT is used for the computation. Cloud elements in an arc cloud are connected with a heavy line. High cloud areas are shaded. Flow patterns are shown with streamlines drawn to fit cloud velocities.

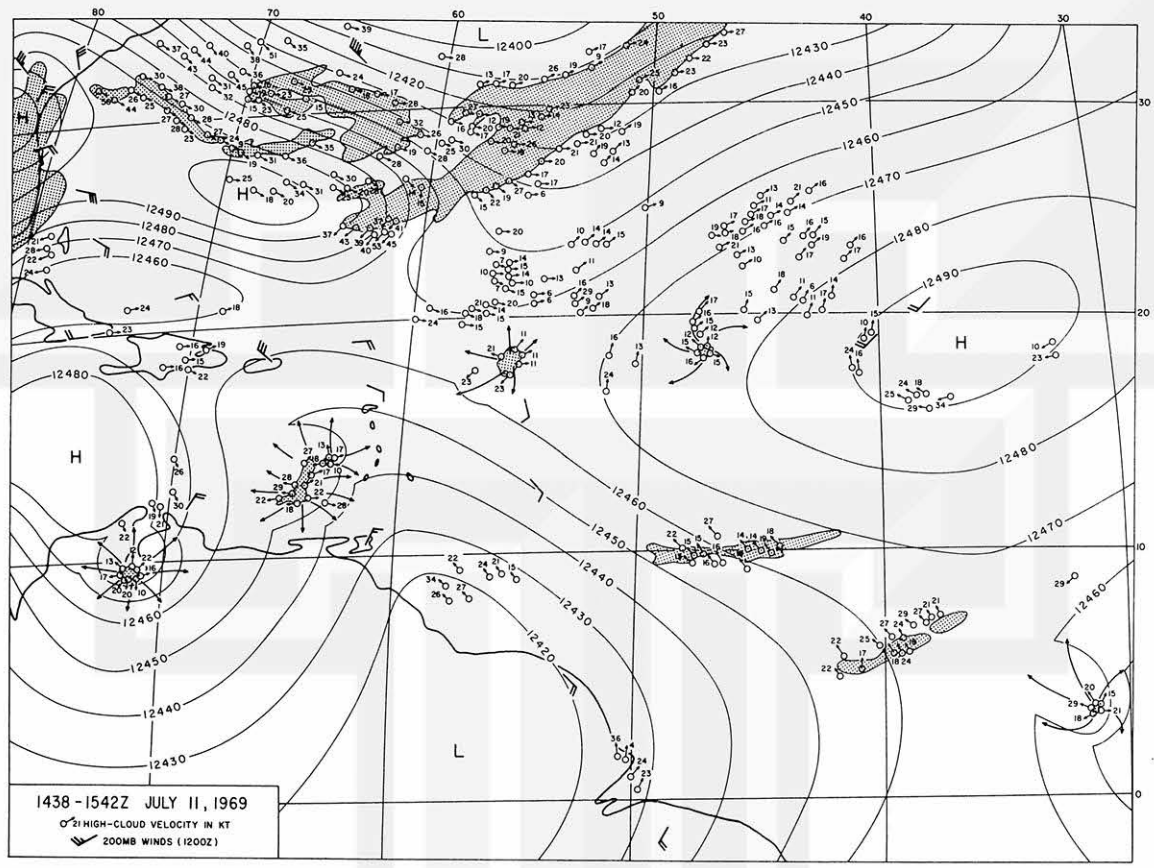

Fig. 14. Velocity vectors of high clouds for the same area shown in Fig. 13 during the same period. Contour lines are drawn using the cloud velocity vectors and the observed 200 mb wind and height data. Streamlines for the expansion high clouds (shaded area) are superimposed.

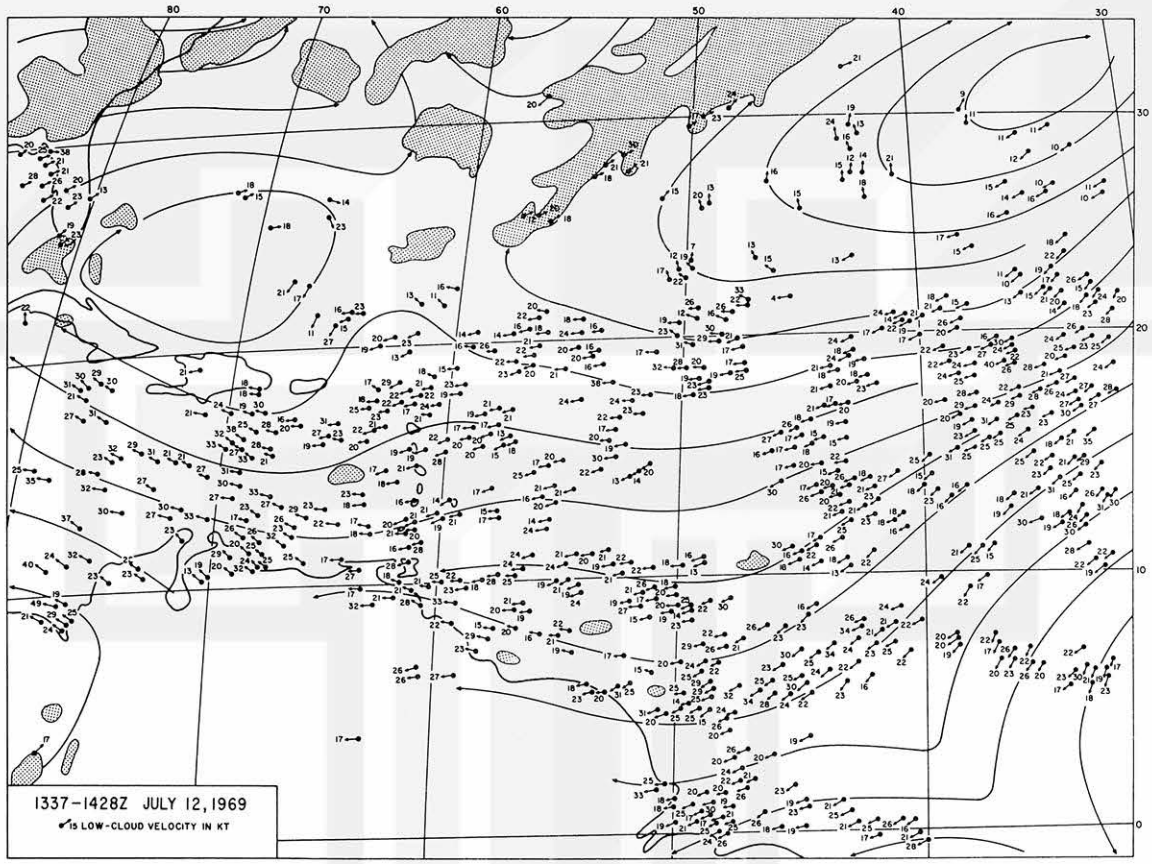

Fig. 15. Velocity vectors of low clouds over the Atlantic Ocean for July 12, 1969. A sequence of six pictures taken between 1337 and 1428 GMT is used for the computation. High cloud areas are shaded. Flow patterns are shown with streamlines drawn to fit cloud velocities.

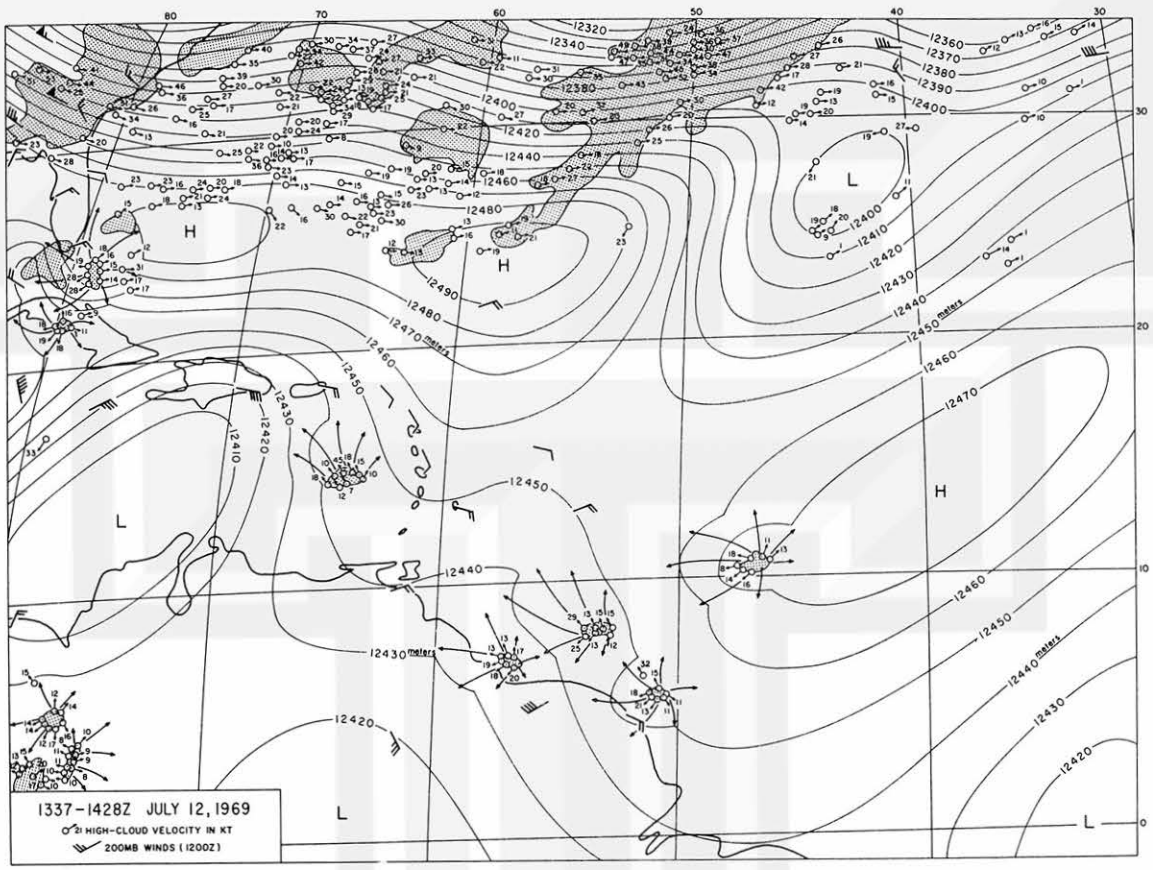

Fig. 16. Velocity vectors of high clouds for the same area shown in Fig. 15 during the same period. Contour lines are drawn using the cloud velocity vectors and the observed 200 mb wind and height data. Streamlines for the expansion high clouds (shaded area) are superimposed.

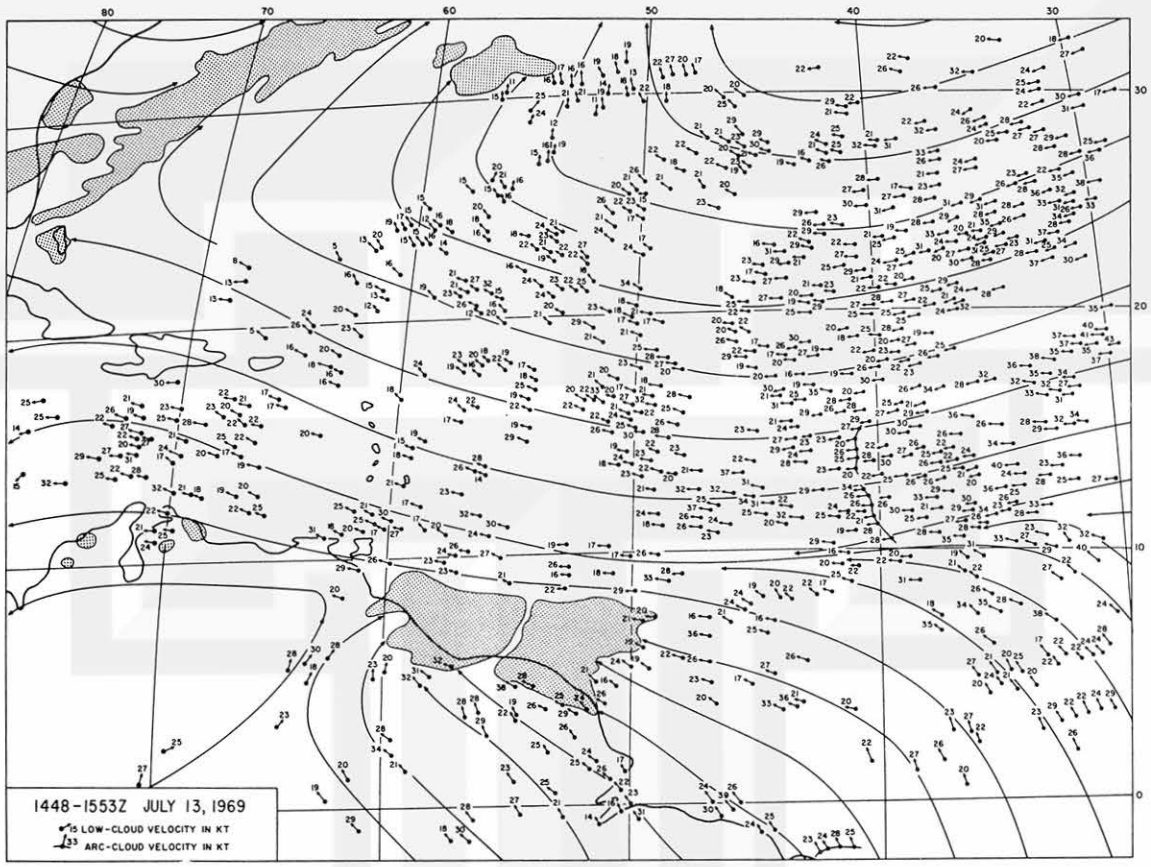

Fig. 17. Velocity vectors of low clouds over the Atlantic Ocean for July 13, 1969. A sequence of six pictures taken between 1448 and 1553 GMT is used for the computation. Cloud elements in an arc cloud are connected with a heavy line. High cloud areas are shaded. Flow patterns are shown with streamlines drawn to fit cloud velocities.

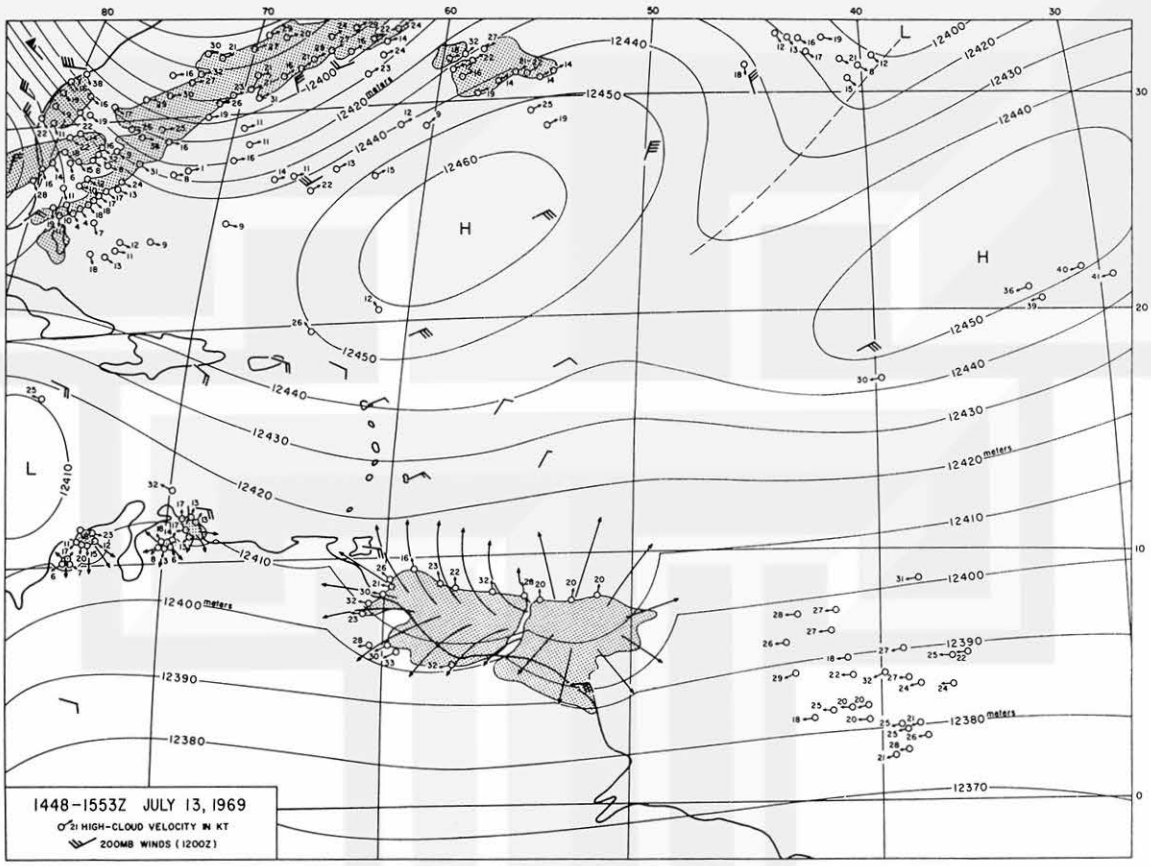

Fig. 18. Velocity vectors of high clouds for the same area shown in Fig. 17 during the same period. Contour lines are drawn using the cloud velocity vectors and the observed 200 mb wind and height data. Streamlines for the expansion high clouds (shaded area) are superimposed.

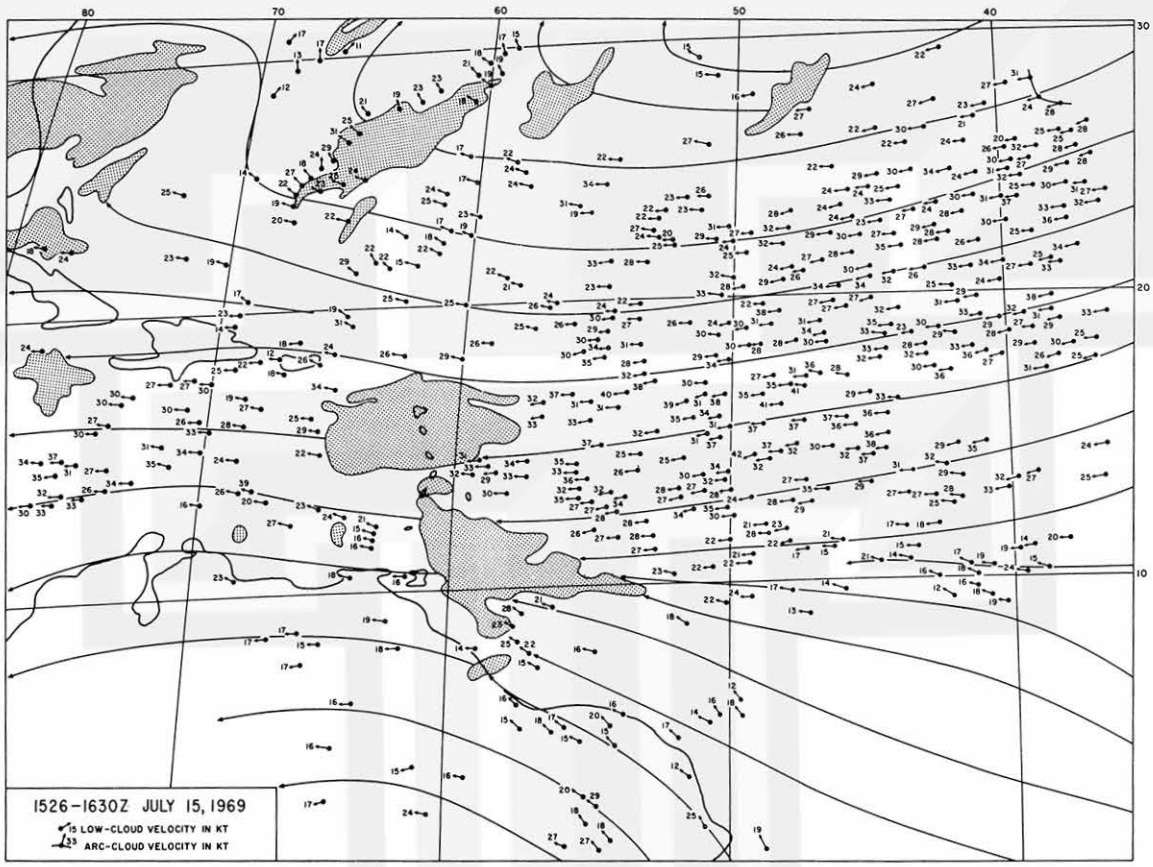

Fig. 19. Velocity vectors of low clouds over the Atlantic Ocean for July 15, 1969. A sequence of six pictures taken between 1526 and 1630 GMT is used for the computation. Cloud elements in an arc cloud are connected with a heavy line. High cloud areas are shaded. Flow patterns are shown with streamlines drawn to fit cloud velocities.

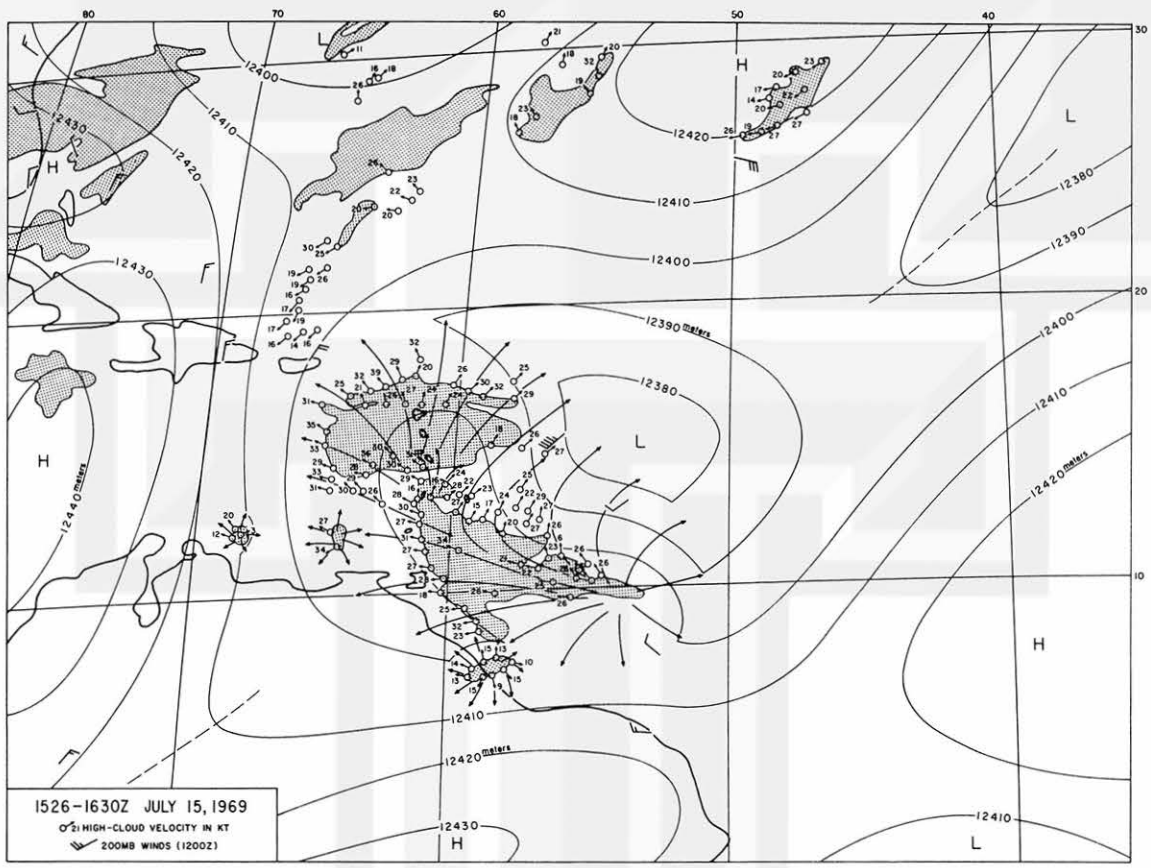

Fig. 20. Velocity vectors of high clouds for the same area shown in Fig. 19 during the same period. Contour lines are drawn using the cloud velocity vectors and the observed 200 mb wind and height data. Streamlines for the expansion high clouds (shaded area) are superimposed.

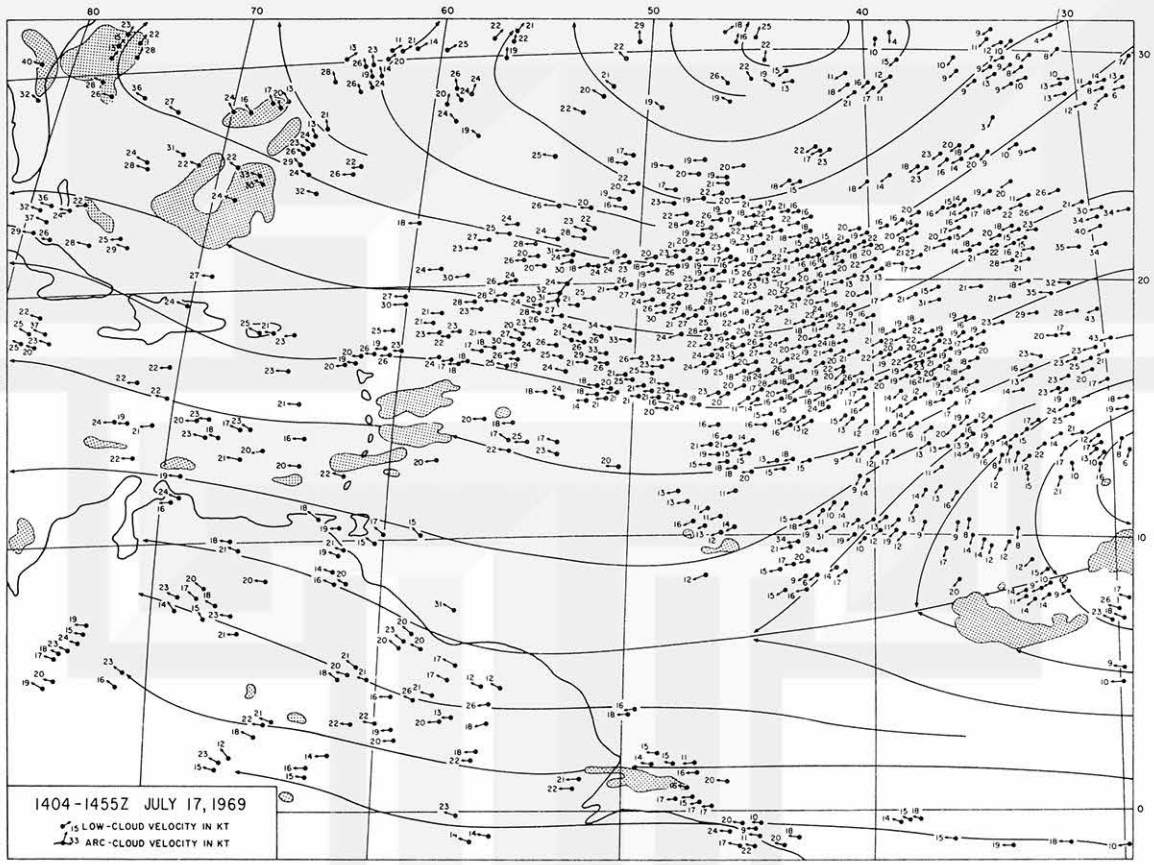

Fig. 21. Velocity vectors of low clouds over the Atlantic Ocean for July 17, 1969. A sequence of five pictures taken between 1404 and 1455 GMT is used for the computation. Cloud elements in an arc cloud are connected with a heavy line. High cloud areas are shaded. Flow patterns are shown with streamlines drawn to fit cloud velocities.

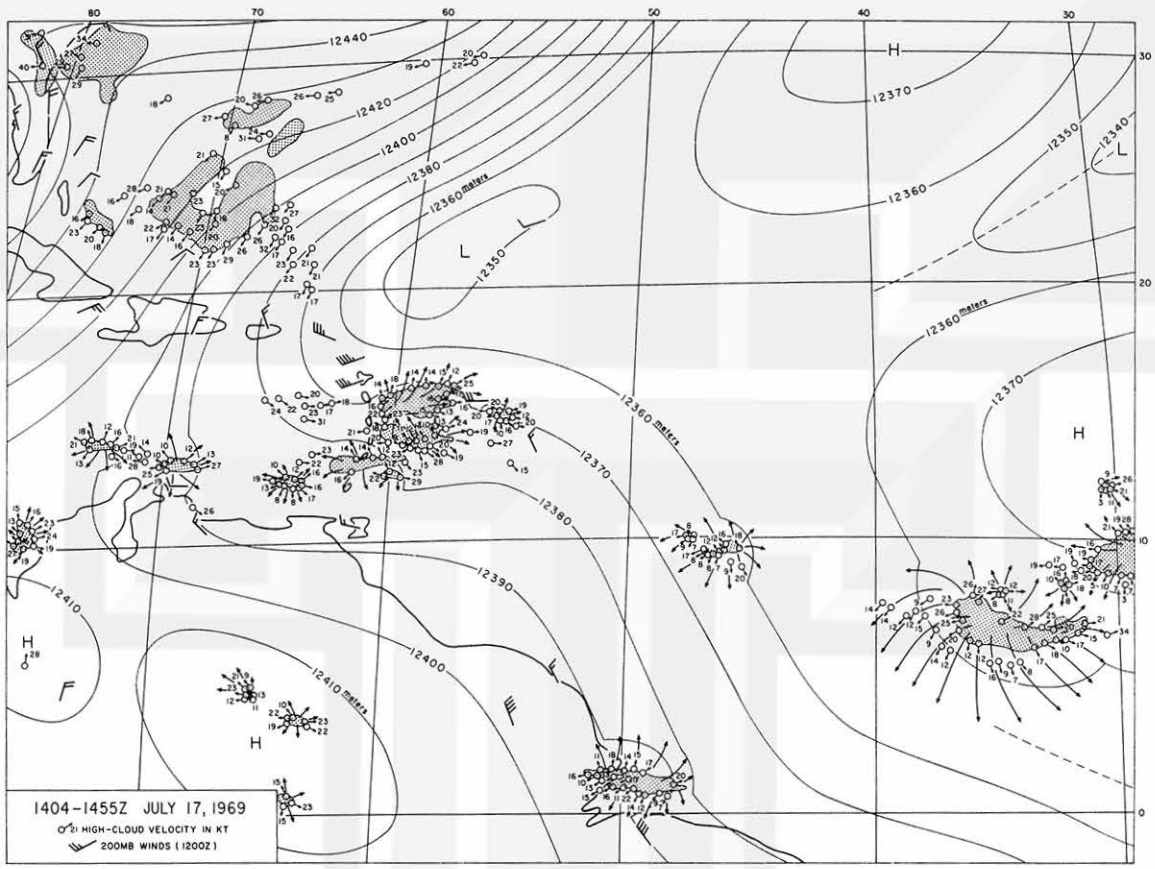

Fig. 22. Velocity vectors of high clouds for the same area shown in Fig. 21 during the same period. Contour lines are drawn using the cloud velocity vectors and the observed 200 mb wind and height data. Streamlines for the expansion high clouds (shaded area) are superimposed.

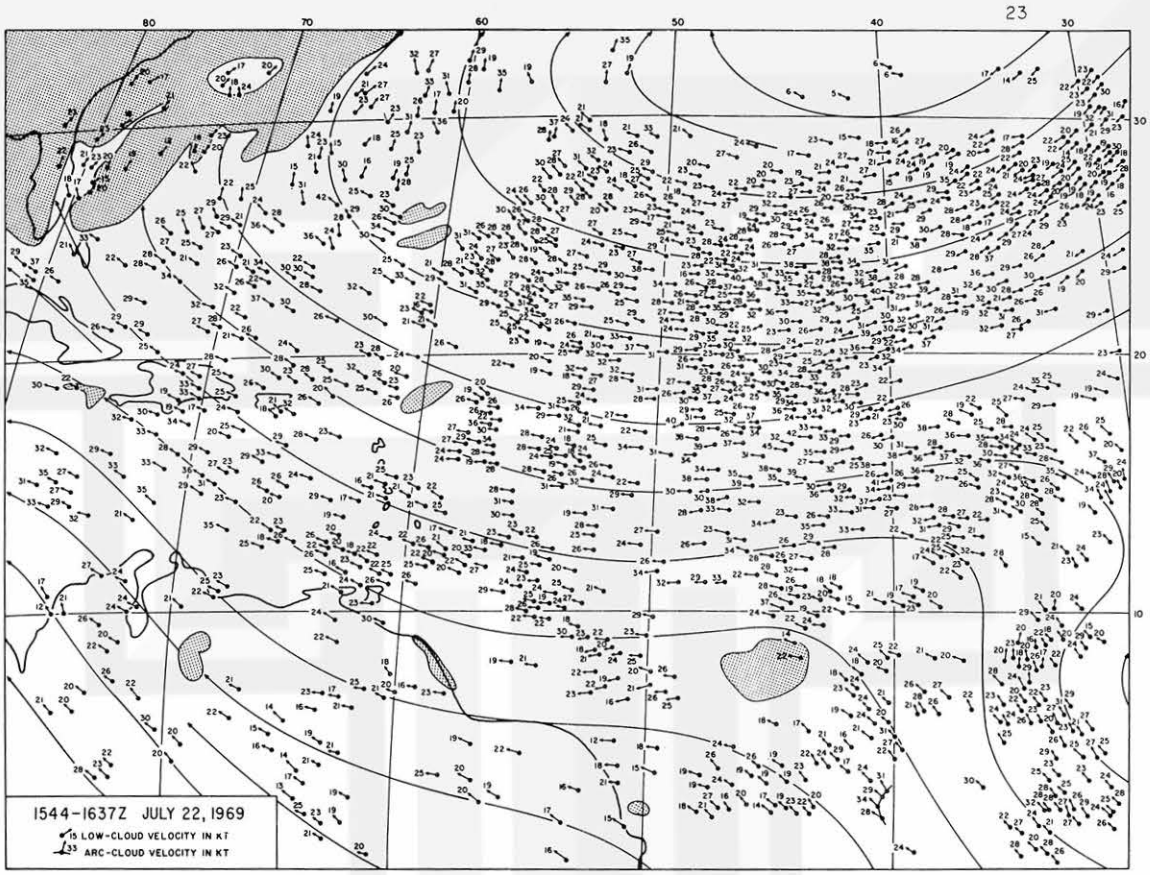

Fig. 23. Velocity vectors of low clouds over the Atlantic Ocean for July 22, 1969. A sequence of five pictures taken between 1544 and 1637 GMT is used for the computation. Cloud elements in an arc cloud are connected with a heavy line. High cloud areas are shaded. Flow patterns are shown with streamlines drawn to fit cloud velocities.

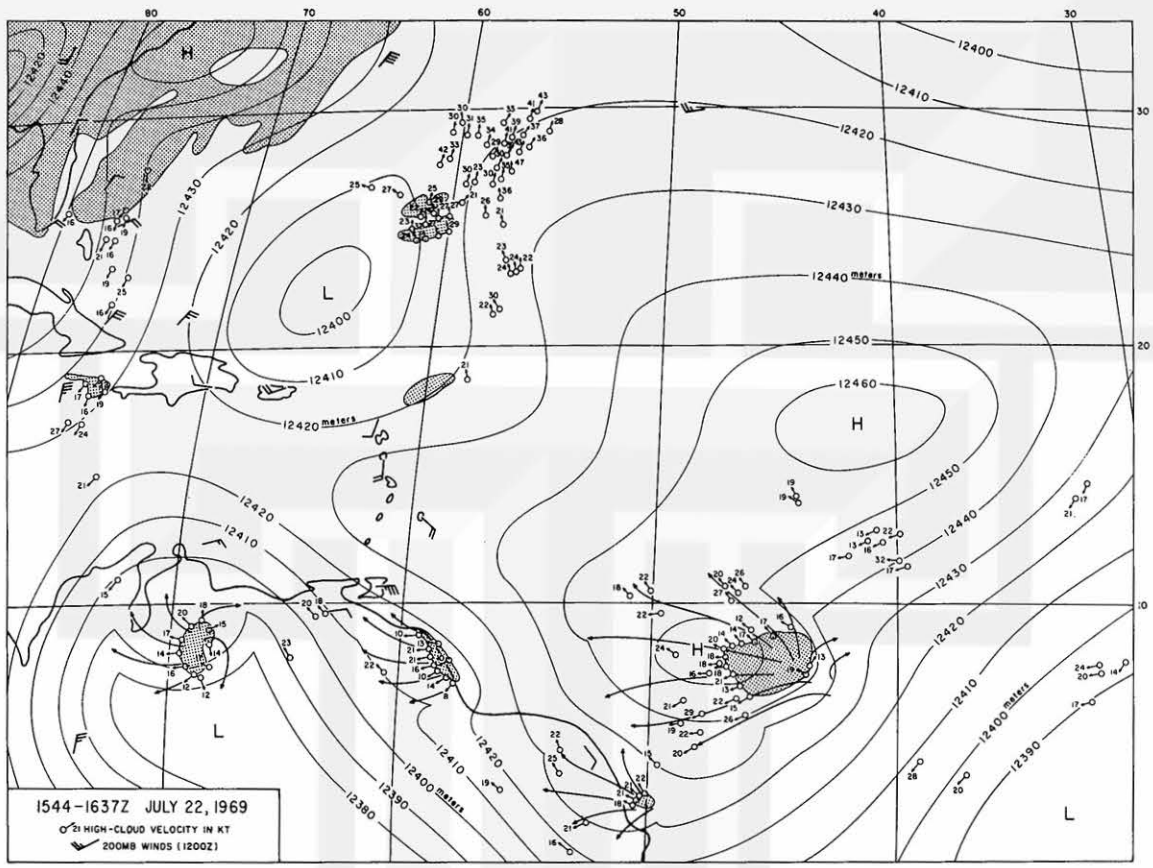

Fig. 24. Velocity vectors of high clouds for the same area shown in Fig. 23 during the same period. Contour lines are drawn using the cloud velocity vectors and the observed 200 mb wind and height data. Streamlines for the expansion high clouds (shaded area) are superimposed.

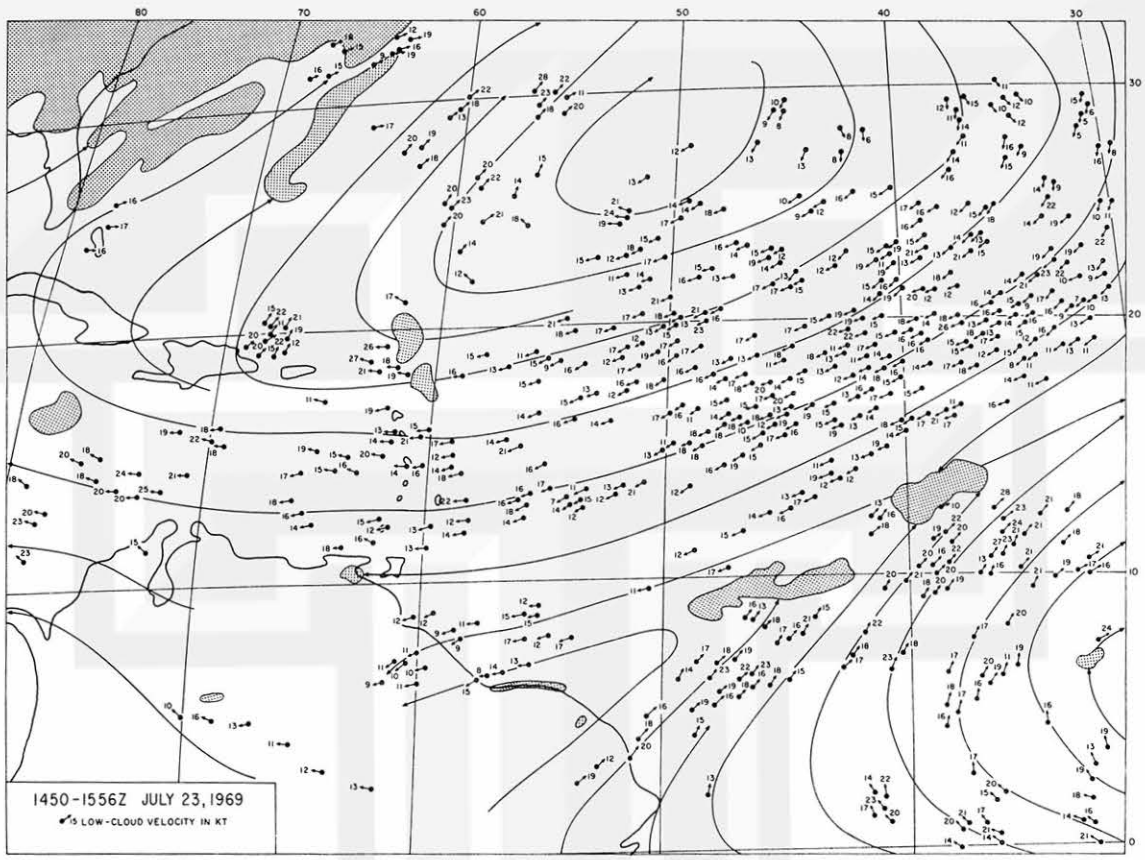

Fig. 25. Velocity vectors of low clouds over the Atlantic Ocean for July 23, 1969. A sequence of six pictures taken between 1450 and 1556 GMT is used for the computation. High cloud areas are shaded. Flow patterns are shown with streamlines drawn to fit cloud velocities.

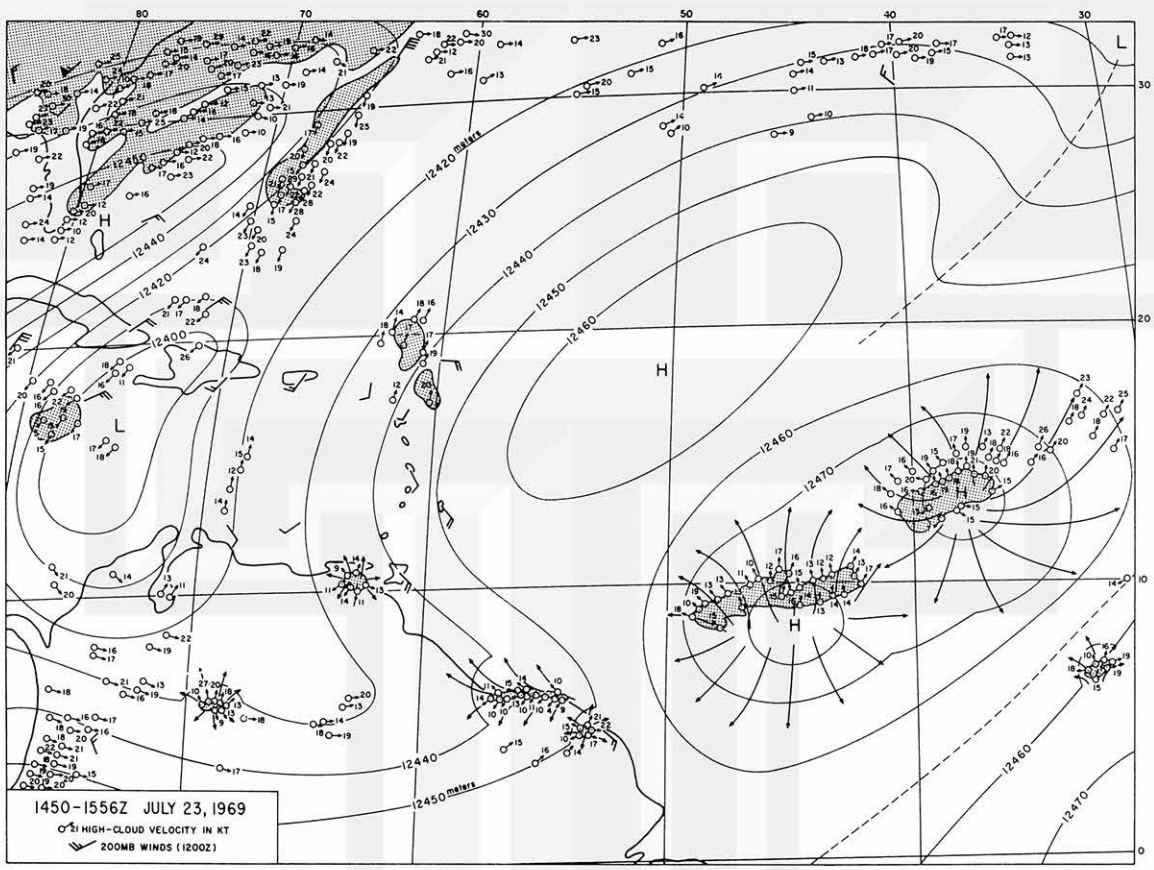

Fig. 26. Velocity vectors of high clouds for the same area shown in Fig. 25 during the same period. Contour lines are drawn using the cloud velocity vectors and the observed 200 mb wind and height data. Streamlines for the expansion high clouds (shaded area) are superimposed.

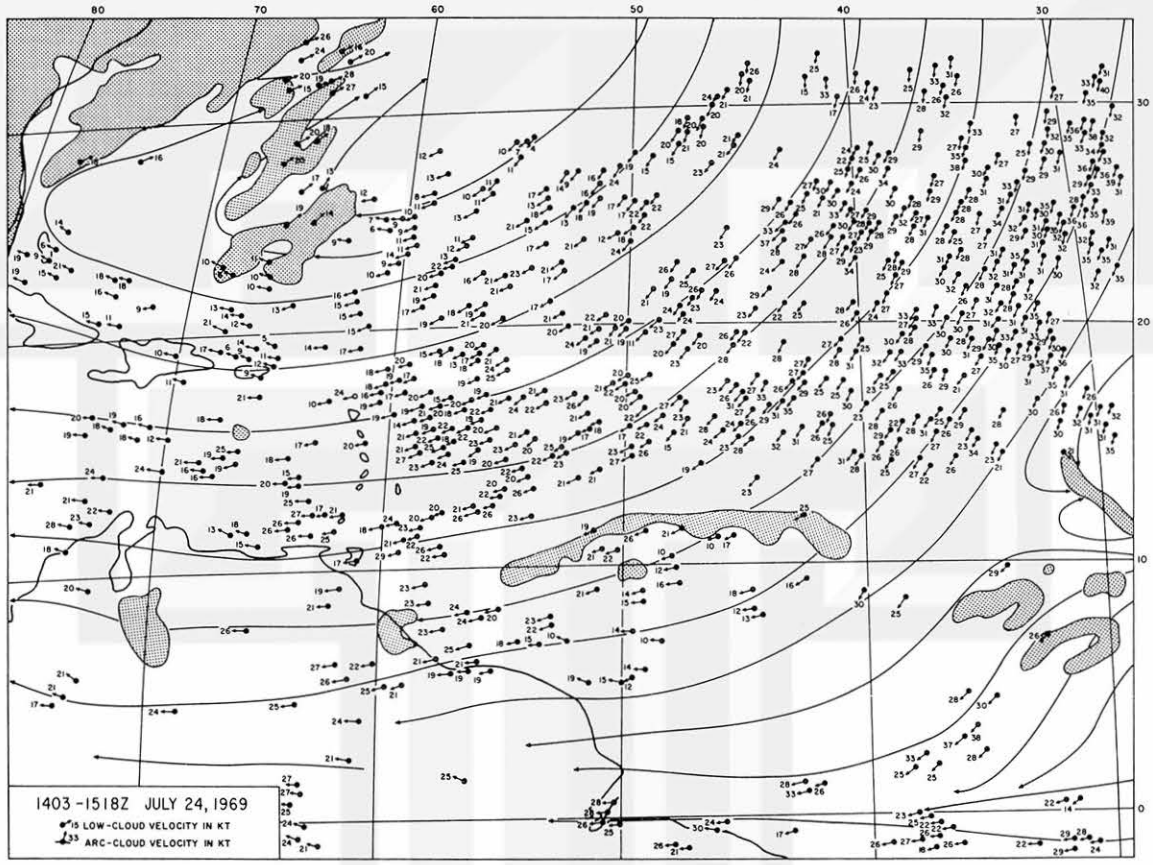

Fig. 27. Velocity vectors of low clouds over the Atlantic Ocean for July 24, 1969. A sequence of six pictures taken between 1405 and 1518 GMT is used for the computation. Cloud elements in an arc cloud are connected with a heavy line. High cloud areas are shaded. Flow patterns are shown with streamlines drawn to fit cloud velocities.

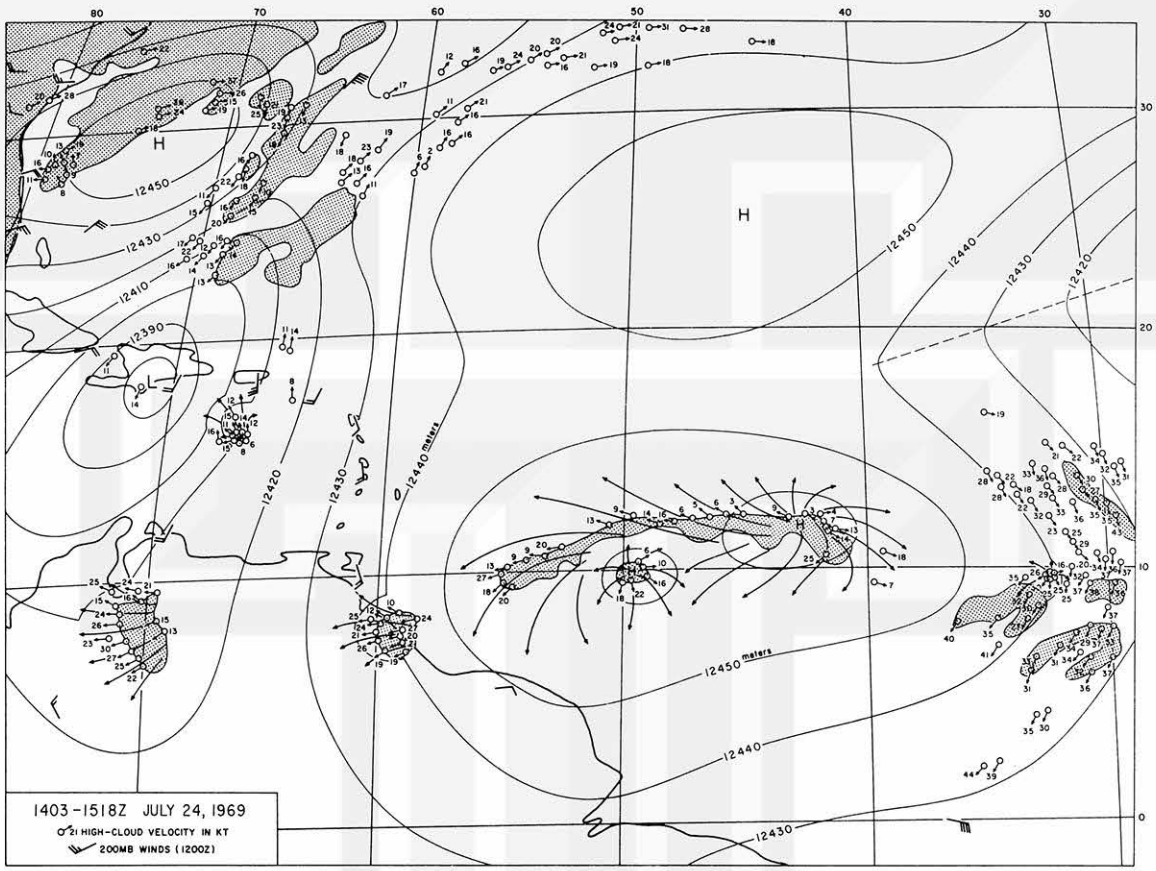

Fig. 28. Velocity vectors of high clouds for the same area shown in Fig. 27 during the same period. Contour lines are drawn using the cloud velocity vectors and the observed 200 mb wind and height data. Streamlines for the expansion high clouds (shaded area) are superimposed.

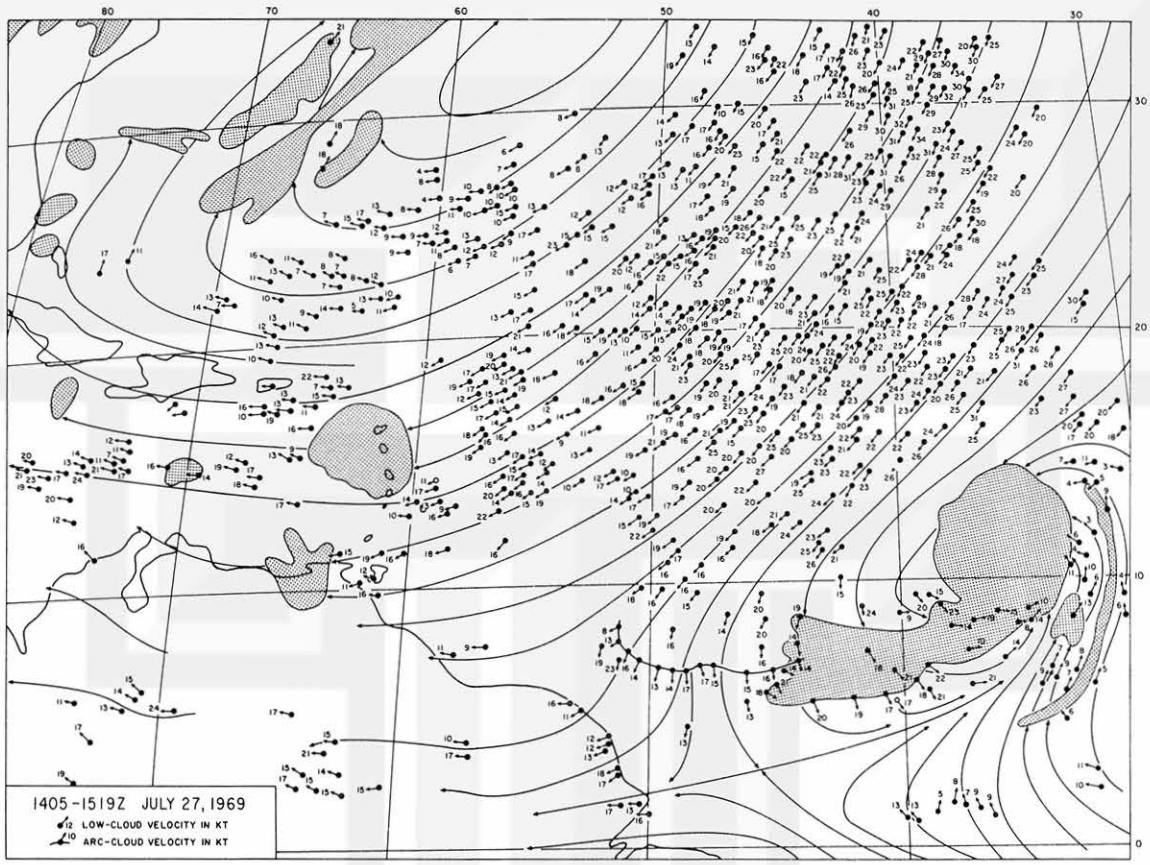

Fig. 29. Velocity vectors of low clouds over the Atlantic Ocean for July 27, 1969. A sequence of six pictures taken between 1405 and 1519 GMT is used for the computation. Cloud elements in an arc cloud are connected with a heavy line. High cloud areas are shaded. Flow patterns are shown with streamlines drawn to fit cloud velocities.

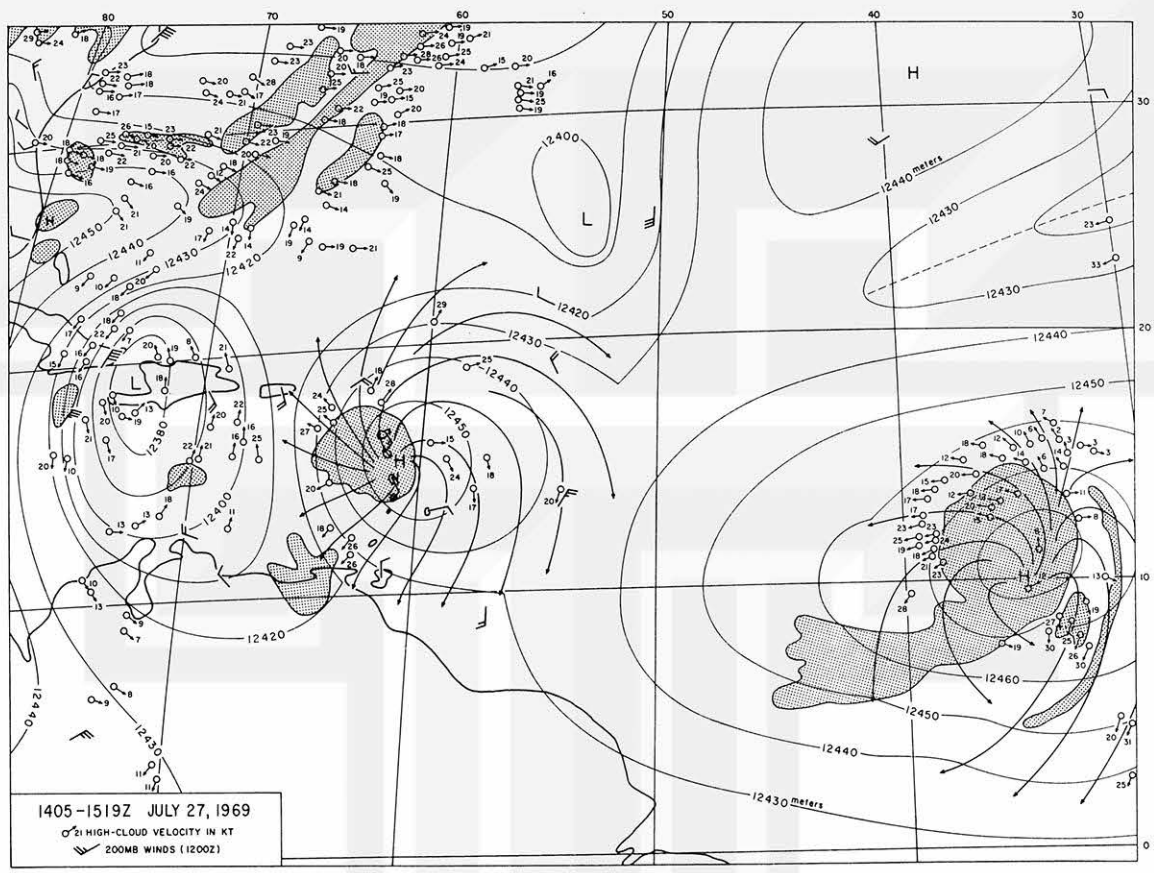

Fig. 30. Velocity vectors of high clouds for the same area shown in Fig. 29 during the same period. Contour lines are drawn using the cloud velocity vectors and the observed 200 mb wind and height data. Streamlines for the expansion high clouds (shaded area) are superimposed.

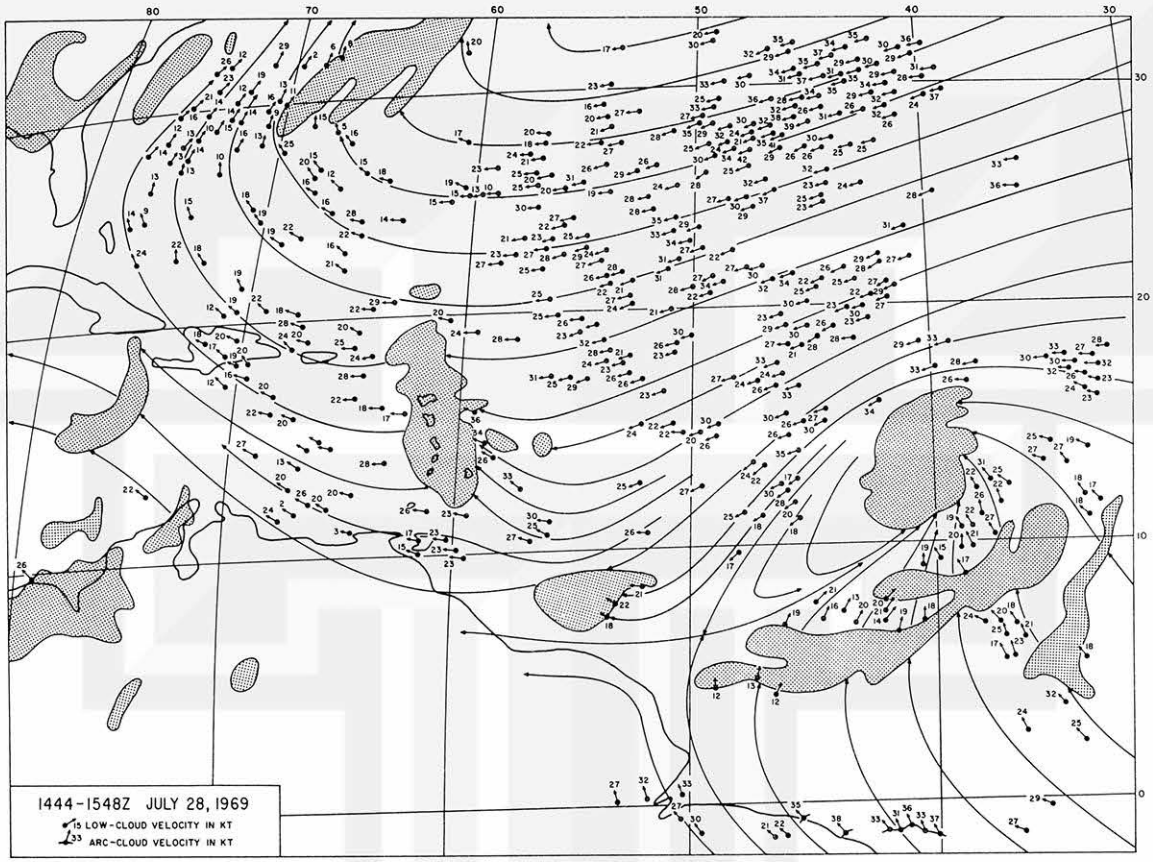

Fig. 31. Velocity vectors of low clouds over the Atlantic Ocean for July 28, 1969. A sequence of six pictures taken between 1444 and 1548 GMT is used for the computation. Cloud elements in an arc cloud are connected with a heavy line. High cloud areas are shaded. Flow patterns are shown with streamlines drawn to fit cloud velocities.

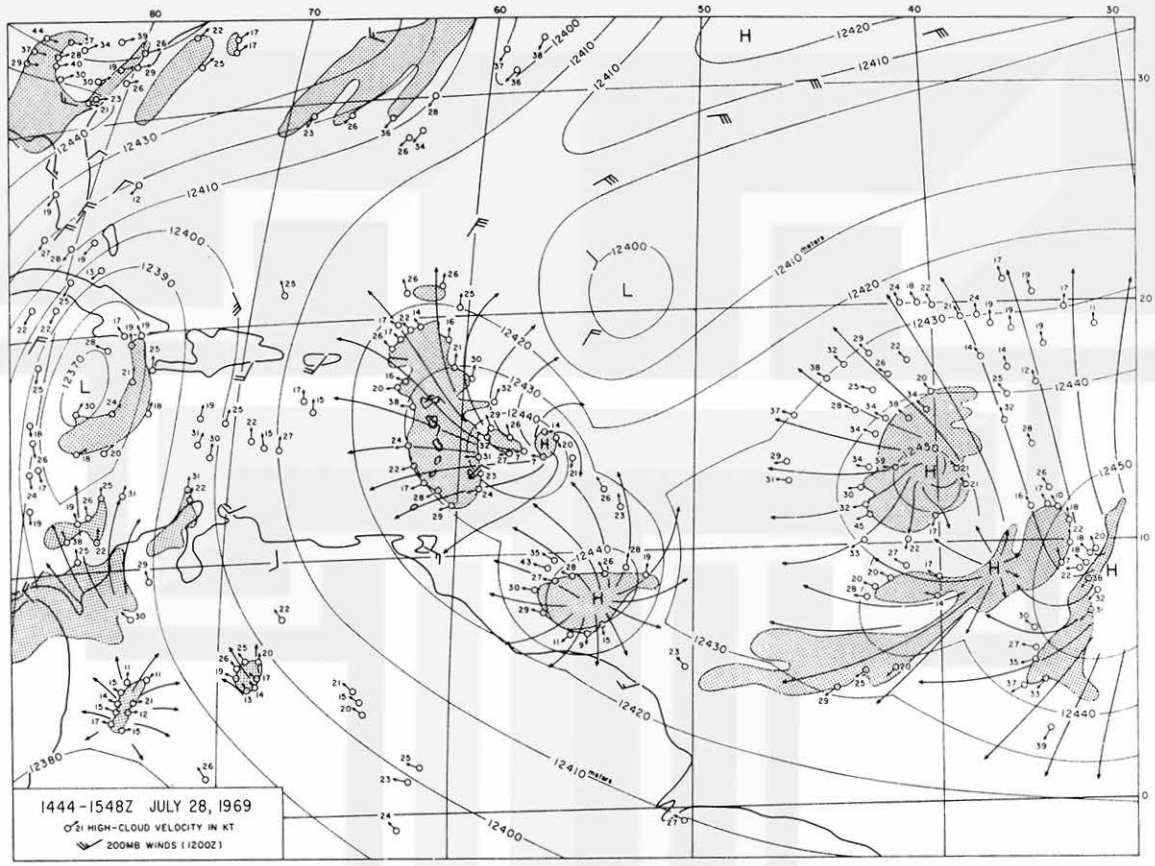

Fig. 32. Velocity vectors of high clouds for the same area shown in Fig. 31 during the same period. Contour lines are drawn using the cloud velocity vectors and the observed 200 mb wind and height data. Streamlines for the expansion high clouds (shaded area) are superimposed.

REFERENCES

Black, P. G. and R. A. Anthes (1971): On the Asymmetric Structure of the Tropical Cyclone Outflow Layer. Journal of Atmospheric Sciences, 28, 1348-1366.

Chang, Y. M., J. J. Tecson and T. T. Fujita (1973): METRACOM System of Cloud Velocity Determination from Geostationary Satellite Pictures. SMRP Research Paper 110, The University of Chicago.

Fernandez-Partagas, J. J. and M. A. Estoque (1970): A Preliminary Report on Meteorological Conditions during Bomex, Fourth Phase (July 11-28, 1969). Rosenstiel School of Marine and Atmospheric Sciences, University of Miami.

Fujita, T. T., D. L. Bradbury, C. Murino and L. Hull (1968): A Study of Mesoscale Cloud Motions Computed from ATS I and Terrestrial Photographs. SMRP Research Paper 71, The University of Chicago.

_____, K. Watanabe and T. Izawa (1969): Formation and Structure of Equatorial Anticyclones Caused by Large-Scale Cross-Equatorial Flow Determined by ATS-I Photographs. Journal of Applied Meteorology, 8, 649-667.

_____ (1970): Application of ATS III Photographs for Determination of Dust and Cloud Velocities over the Northern Tropical Atlantic. SMRP Research Paper 90, The University of Chicago.

_____, E. W. Pearl and W. E. Shenk (1973): Satellite-Tracked Cumulus Velocities. SMRP Research Paper 114, The University of Chicago.

_____ (1974): Overshooting Thunderheads Observed from ATS and Learjet. SMRP Research Paper 117, The University of Chicago.

Gaby, D. C. and K. O. Poteat (1973): ATS-3 Satellite-Derived Low-Level Winds: A Provisional Climatology. Journal of Applied Meteorology, 12, 1054-1061.

Kurihara, Y. and R. E. Tuleya (1974): Structure of a Tropical Cyclone Developed in a Three-Dimensional Numerical Simulation Model. Journal of Atmospheric Sciences, 31, 893-919.

Riehl, H. (1954): Tropical Meteorology. McGraw-Hill, New York.

MESOMETEOROLOGY PROJECT - - - RESEARCH PAPERS

(Continued from front cover)

42.* A Study of Factors Contributing to Dissipation of Energy in a Developing Cumulonimbus - Rodger A. Brown and Tetsuya Fujita

43. A Program for Computer Gridding of Satellite Photographs for Mesoscale Research - William D. Bonner

44. Comparison of Grassland Surface Temperatures Measured by TIROS VII and Airborne Radiometers under Clear Sky and Cirriform Cloud Conditions - Ronald M. Reap

45. Death Valley Temperature Analysis Utilizing Nimbus I Infrared Data and Ground-Based Measurements - Ronald M. Reap and Tetsuya Fujita

46. On the "Thunderstorm-High Controversy" - Rodger A. Brown

47. Application of Precise Fujita Method on Nimbus I Photo Gridding - Lt. Cmd. Ruben Nasta

48. A Proposed Method of Estimating Cloud-top Temperature, Cloud Cover, and Emissivity and Whiteness of Clouds from Short- and Long-wave Radiation Data Obtained by TIROS Scanning Radiometers - T. Fujita and H. Grandoso

49. Aerial Survey of the Palm Sunday Tornadoes of April 11, 1965 - Tetsuya Fujita

50. Early Stage of Tornado Development as Revealed by Satellite Photographs - Tetsuya Fujita

51. Features and Motions of Radar Echoes on Palm Sunday, 1965 - D. L. Bradbury and T. Fujita

52. Stability and Differential Advection Associated with Tornado Development - Tetsuya Fujita and Dorothy L. Bradbury

53. Estimated Wind Speeds of the Palm Sunday Tornadoes - Tetsuya Fujita

54. On the Determination of Exchange Coefficients: Part II - Rotating and Nonrotating Convective Currents - Rodger A. Brown

55. Satellite Meteorological Study of Evaporation and Cloud Formation over the Western Pacific under the Influence of the Winter Monsoon - K. Tsuchiya and T. Fujita

56. A Proposed Mechanism of Snowstorm Mesojet over Japan under the Influence of the Winter Monsoon - T. Fujita and K. Tsuchiya

57. Some Effects of Lake Michigan upon Squall Lines and Summertime Convection - Walter A. Lyons

58. Angular Dependence of Reflection from Stratiform Clouds as Measured by TIROS IV Scanning Radiometers - A. Rabbe

59. Use of Wet-beam Doppler Winds in the Determination of the Vertical Velocity of Raindrops inside Hurricane Rainbands - T. Fujita, P. Black and A. Loesch

60. A Model of Typhoons Accompanied by Inner and Outer Rainbands - Tetsuya Fujita, Tatsuo Izawa,, Kazuo Watanabe and Ichiro Imai

61. Three-Dimensional Growth Characteristics of an Orographic Thunderstorm System - Rodger A. Brown

62. Split of a Thunderstorm into Anticyclonic and Cyclonic Storms and their Motion as Determined from Numerical Model Experiments - Tetsuya Fujita and Hector Grandoso

63. Preliminary Investigation of Peripheral Subsidence Associated with Hurricane Outflow - Ronald M. Reap

64. The Time Change of Cloud Features in Hurricane Anna, 1961, from the Easterly Wave Stage to Hurricane Dissipation - James E. Arnold

65. Easterly Wave Activity over Africa and in the Atlantic with a Note on the Intertropical Convergence Zone during Early July 1961 - James E. Arnold

66. Mesoscale Motions in Oceanic Stratus as Revealed by Satellite Data - Walter A. Lyons and Tetsuya Fujita

67. Mesoscale Aspects of Orographic Influences on Flow and Precipitation Patterns - Tetsuya Fujita

68. A Mesometeorological Study of a Subtropical Mesocyclone -Hidetoshi Arakawa, Kazuo Watanabe, Kiyoshi Tsuchiya and Tetsuya Fujita

69. Estimation of Tornado Wind Speed from Characteristic Ground Marks - Tetsuya Fujita, Dorothy L. Bradbury and Peter G. Black

70. Computation of Height and Velocity of Clouds from Dual, Whole-Sky, Time-Lapse Picture Sequences - Dorothy L. Bradbury and Tetsuya Fujita

71. A Study of Mesoscale Cloud Motions Computed from ATS-I and Terrestrial Photographs - Tetsuya Fujita, Dorothy L. Bradbury, Clifford Murino and Louis Hull

72. Aerial Measurement of Radiation Temperatures over Mt. Fuji and Tokyo Areas and Their Application to the Determination of Ground- and Water-Surface Temperatures - Tetsuya Fujita, Gisela Baralt and Kiyoshi Tsuchiya

73. Angular Dependence of Reflected Solar Radiation from Sahara Measured by TIROS VII in a Torquing Maneuver - Rene Mendez.

74. The Control of Summertime Cumuli and Thunderstorms by Lake Michigan During Non-Lake Breeze Conditions - Walter A. Lyons and John W. Wilson

75. Heavy Snow in the Chicago Area as Revealed by Satellite Pictures - James Bunting and Donna Lamb

76. A Model of Typhoons with Outflow and Subsidence Layers - Tatsuo Izawa

* out of print

(continued on outside back cover)

77. Yaw Corrections for Accurate Gridding of Nimbus HRIR Data - R. A. Madden
78. Formation and Structure of Equatorial Anticyclones caused by Large-Scale Cross Equatorial Flows determined by ATS I Photographs - T. T. Fujita, K. Watanabe and T. Izawa
79. Determination of Mass Outflow from a Thunderstorm Complex using ATS III Pictures - T. T. Fujita and D. L. Bradbury
80. Development of a Dry Line as shown by ATS Cloud Photography and verified by Radar and Conventional Aerological Data - D. L. Bradbury
81. Dynamical Analysis of Outflow from Tornado-Producing Thunderstorms as revealed by ATS III Pictures - K. Ninomiya
*82. Computation of Cloud Heights from Shadow Positions through Single Image Photogrammetry of Apollo Pictures - T. T. Fujita
83. Aircraft, Spacecraft, Satellite and Radar Observations of Hurricane Gladys, 1968 - R. C. Gentry, T. Fujita and R. C. Sheets
84. Basic Problems on Cloud Identification related to the design of SMS-GOES Spin Scan Radiometers - T. T. Fujita
85. Mesoscale Modification of Synoptic Situations over the Area of Thunderstorms' Development as revealed by ATS III and Aerological Data - K. Ninomiya
86. Palm Sunday Tornadoes of April 11, 1965 - T. T. Fujita, D. L. Bradbury and C. F. Van Thullenar (Reprinted from Mon. Wea. Rev., 98, 29-69, 1970)
87. Patterns of Equivalent Blackbody Temperature and Reflectance of Model Clouds computed by changing Radiometer's Field of View - J. J. Tecson
88. Lubbock Tornadoes of 11 May 1970 - T. T. Fujita
89. Estimate of Areal Probability of Tornadoes from Inflationary Reporting of their Frequencies - T. T. Fujita
90. Application of ATS III Photographs for determination of Dust and Cloud Velocities over Northern Tropical Atlantic - T. T. Fujita
91. A Proposed Characterization of Tornadoes and Hurricanes by Area and Intensity - T. T. Fujita
92. Estimate of Maximum Wind Speeds of Tornadoes in Three Northwestern States - T. T. Fujita
93. In- and Outflow Field of Hurricane Debbie as revealed by Echo and Cloud Velocities from Airborne Radar and ATS-III Pictures - T. T. Fujita and P. G. Black (Reprinted from Preprint of Radar Meteorology Conference, Nov. 17-20, 1970, Tucson, Arizona)
94. Characterization of 1965 Tornadoes by their Area and Intensity - J. J. Tecson
*95. Computation of Height and Velocity of Clouds over Barbados from a Whole-Sky Camera Network - R. D. Lyons
96. The Filling over Land of Hurricane Camille, August 17-18, 1969 - D. L. Bradbury
97. Tornado Occurrences related to Overshooting Cloud-Top Heights as determined from ATS Pictures - T. T. Fujita
98. F P P Tornado Scale and its Applications - T. T. Fujita and A. D. Pearson
99. Preliminary Results of Tornado Watch Experiment 1971 - T. T. Fujita, J. J. Tecson and L. A. Schaal
100. F-Scale Classification of 1971 Tornadoes - T. T. Fujita
101. Typhoon-Associated Tornadoes in Japan and new evidence of Suction Vortices in a Tornado near Tokyo - T. T. Fujita
102. Proposed Mechanism of Suction Spots accompanied by Tornadoes - T. T. Fujita
103. A Climatological Study of Cloud Formation over the Atlantic during Winter Monsoon - H. Shitara
**104. Statistical Analysis of 1971 Tornadoes - E. W. Pearl
105. Estimate of Maximum Windspeeds of Tornadoes in Southernmost Rockies - T. T. Fujita
106. Use of ATS Pictures in Hurricane Modification - T. T. Fujita
107. Mesoscale Analysis of Tropical Latin America - T. T. Fujita
108. Tornadoes Around The World - T. T. Fujita (Reprinted from Weatherwise, 26, No. 2, April 1973)
109. A Study of Satellite-Observed Cloud Patterns of Tropical Cyclones - E. E. Balogun
110. METRACOM System of Cloud-Velocity determination from Geostationary Satellite Pictures - Y. M. Chang, J. J. Tecson and T. T. Fujita
111. Proposed Mechanism of Tornado Formation from Rotating Thunderstorm - T. T. Fujita
112. Joliet Tornado of April 6, 1972 - E. W. Pearl
113. Results of F P P Classification of 1971 and 1972 Tornadoes - T. T. Fujita and A. D. Pearson
114. Satellite-Tracked Cumulus Velocities - T. T. Fujita, E. W. Pearl and W. E. Shenk
115. General and Local Circulation of Mantle and Atmosphere toward Prediction of Earthquakes and Tornadoes - T. T. Fujita and K. Fujita
116. Cloud Motion Field of Hurricane Ginger during the Seeding Period as determined by the METRACOM System - J. J. Tecson, Y. M. Chang and T. T. Fujita
117. Overshooting Thunderheads observed from ATS and Learjet - T. T. Fujita
118. Thermal and Dynamical Features of a Thunderstorm with a Tilted Axis of Rotation - T. T. Fujita
119. Characteristics of Anvil-Top Associated with the Poplar Bluff Tornado of May 7, 1973 - E. W. Pearl
120. Jumbo Tornado Outbreak of 3 April 1974 - T. T. Fujita